JAERI-M
83-059

OPTIMUM CONFIGURATION AND OPERATION REGIME OF PUMPED LIMITER IN INTOR

April 1983

Masayoshi SUGIHARA, Seiji SAITO*,
Noboru FUJISAWA and Nobuharu MIKI**

日本原子力研究所
Japan Atomic Energy Research Institute

JAERI-M レポートは，日本原子力研究所が不定期に公刊している研究報告書です。
入手の問合わせは，日本原子力研究所技術情報部情報資料課（〒319—11 茨城県那珂郡東海村）あて，お申しこしください。なお，このほかに財団法人原子力弘済会資料センター（〒319—11 茨城県那珂郡東海村日本原子力研究所内）で複写による実費頒布をおこなっております。

JAERI-M reports are issued irregularly.
Inquiries about availability of the reports should be addressed to Information Section, Division of Technical Information, Japan Atomic Energy Research Institute, Tokai-mura, Naka-gun, Ibaraki-ken 319-11, Japan.

編集兼発行　日本原子力研究所
印　　刷　日立高速印刷株式会社

JAERI-M 83-059

Optimum Configuration and Operation Regime of Pumped Limiter in INTOR

Masayoshi SUGIHARA, Seiji SAITO*, Noboru FUJISAWA and Nobuharu MIKI**

Division of Large Tokamak Development,
Tokai Research Establishment, JAERI

(Received March 8, 1983)

A detailed recycling model of neutral particles on the limiter surface and first wall in the one-dimensional tokamak transport code are developed. The energy of neutral particles, which flow back from the limiter chamber, is calculated by the two-dimensional Monte-Carlo neutral code, and is incorporated into the tokamak code. The optimum configuration and operation regime of the pumped limiter in INTOR are obtained. The main conclusions obtained are (1) the electron temperature in the scrape-off layer plasma decays rapidly, while the density distribution is fairly broad, (2) a considerably long limiter with a moderate pumping speed is sufficient to keep the helium accumulation in the main plasma at a desired level, (3) overall particle confinement time for helium becomes much longer than that for fuel particles, (4) the minimum amount of tritium pumped out little depends on the limiter length, if the pumping speed is appropriately adjusted so as to keep the helium accumulation at the same level, (5) the electron temperature at the boundary is 400 ∿ 500 eV when the fueling is performed by the realistic pellet injection or gas-puffing, (6) although the high temperature operation regime (700 ∿ 900 eV) can be realized by large pumping and ideal pellet injection with short limiter length, this regime will not necessarily be preferable if the heat flux and erosion of the leading edge are more critical for the engineering.

Keywords: Pumped Limiter, Tokamak Reactor, One-dimensional Transport Code, Particle Recycling, Helium Exhaust, Heat Load, Erosion

---

* On leave from Hitachi Ltd., Hitachi
** Toshiba Corporation, Yokohama

JAERI−M 83−059

ＩＮＴＯＲのポンプリミタの最適形状および動作領域

日本原子力研究所東海研究所大型トカマク開発部
杉原　正芳・斎藤　誠次*・藤沢　　登・三木　信晴**

（１９８３年３月８日受理）

トカマク核融合炉のポンプリミタの最適形状および動作領域を求めるため，一次元トカマク輸送コードにおけるリミタ面，第一壁面上での中性粒子の詳細なリサイクリングモデルを開発した。ポンプリミタチャンバーから主プラズマ側へ戻る中性粒子エネルギーを二次元モンテカルロコードで計算して一次元コードに組み込む。主にＩＮＴＯＲを対象として行った解析により得られた主な結果は次のとおりである。(1)スクレープオフ層内の電子温度は急激に減少するが，密度は相当平坦である。(2)それ程大きくないポンプスピードとかなり長いリミタで主プラズマ中のヘリウム蓄積を所定の値に維持することができる。(3)ヘリウムに対する粒子閉じ込め時間は燃料粒子に対するものより相当長い。(4)ポンプスピードを主プラズマのヘリウム蓄積量が同一になるように適当に調整すれば，ポンプに引かれるトリチウムの最小量はリミタの長さに依存しない。(5)燃料供給を現実的なペレット入射かガスパフで行うと境界電子温度は400～500ｅＶ となる。(6)より高温の境界電子温度(700～900ｅＶ) は，理想的なペレットと大排気容量のポンプを用い，リミタ長を短くすることにより実現できるが，もしリミタ先端部の熱負荷や浸食が技術的に最も厳しければ，この動作領域は必ずしも好ましい動作領域ではない。

＊外来研究員，日立製作所
＊＊東京芝浦電気㈱

CONTENTS

1. Introduction 1
2. Calculational Model 2
2.1 Recycling model of neutral particles 2
2.2 Model of one-dimensional transport code 7
3. Results of Calculations 11
3.1 Parameters of scrape-off layer plasma 11
3.2 Helium ash accumulation and exhaust 12
3.3 Heat load and erosion 16
4. Engineering Considerations for the Pumped Limiter 19
5. Conclusions 22
Acknowledgment 25
References 26

目　　次

1. 序　論 1
2. 計算モデル 2
2.1 中性粒子のリサイクリングモデル 2
2.2 一次元トカマク輸送コードのモデル 7
3. 計算結果 11
3.1 スクレープオフ層プラズマのパラメータ 11
3.2 ヘリウム蓄積と排気 12
3.3 熱負荷と浸食 16
4. ポンプリミタの技術的考察 19
5. 結　論 22
謝　辞 25
参考文献 26

1. Introduction

Poloidal divertor system for impurity control and helium ash exhaust in tokamak fusion reactors has been studied extensively [1-5]. It is considered at present that this system has the highest possibility to meet those requirements. However, from the engineering view points, the poloidal divertor system is rather complicated and has some problems in remote maintenance [6]. In addition, the capacity of the electrical power supply for poloidal field coils may become quite large [7].

In order to alleviate these engineering problems, the pumped-limiter concept has been proposed [8-10]. The purpose of this paper is to determine the optimum configuration and operation parameters of the pumped limiter in tokamak fusion reactors, especially in INTOR. Various requirements for pumped limiter and possible methods to meet them are summarized in Table 1. It will be essential to combine these possible methods appropriately to meet these requirements. For instance, it is preferable to install the leading edge of the limiter far from the main plasma to mitigate the heat load and erosion of the edge. If it is installed too far, however, the capability of the helium ash exhaust might be failed.

In order to analyse the optimum configuration and operation regimes of the pumped limiter, we develop a detailed recycling model of neutral particles at the limiter and first wall in the one-dimensional tokamak transport code, which calculates the transport process in the main plasma including the scrape-off layer plasma. In the pumped limiter chamber, the behavior of the neutral particles is calculated by the two-dimensional Monte-Carlo code with fixed parameters of the scrape-off layer plasma, which are given from the one-dimensional tokamak

transport code. The average energy of the neutral particles, which flow back to the main plasma from the limiter chamber, is delivered to the transport code, and the equilibrium state both of main and scrape-off layer plasma is calculated. On the basis of these calculations, optimum configuration and operation regimes of the pumped limiter to meet the requirements in Table 1 is determined with the use of the possible methods in Table 1.

The structure of this paper is as follows. In §2, detailed model of the one-dimensional tokamak transport code is presented. Brief explanation of the two-dimensional Monte-Carlo code for limiter chamber is also presented. In §3, the resutls of calculations are obtained. In §4, engineering considerations are given. In §5, conclusions are drawn.

2. Calculational Model

The schematic drawing of the calculational model is shown in Fig.1. To simplify the drawing, the part of the pumped limiter chamber is somewhat exaggerated. The main plasma including the scrape-off layer plasma from the opening of the pumped limiter chamber is calculated by the one-dimensional tokamak transport code. In the pumped limiter chamber, the behavior of the neutral particles is calculated by the two-dimensional Monte-Carlo code.

2.1 Recycling model of neutral particles

Details of the recycling model of neutral particles at various points on the limiter and wall in the one-dimensional tokamak transport code are as follows.

transport code. The average energy of the neutral particles, which flow back to the main plasma from the limiter chamber, is delivered to the transport code, and the equilibrium state both of main and scrape-off layer plasma is calculated. On the basis of these calculations, optimum configuration and operation regimes of the pumped limiter to meet the requirements in Table 1 is determined with the use of the possible methods in Table 1.

The structure of this paper is as follows. In §2, detailed model of the one-dimensional tokamak transport code is presented. Brief explanation of the two-dimensional Monte-Carlo code for limiter chamber is also presented. In §3, the resutls of calculations are obtained. In §4, engineering considerations are given. In §5, conclusions are drawn.

2. Calculational Model

The schematic drawing of the calculational model is shown in Fig.1. To simplify the drawing, the part of the pumped limiter chamber is somewhat exaggerated. The main plasma including the scrape-off layer plasma from the opening of the pumped limiter chamber is calculated by the one-dimensional tokamak transport code. In the pumped limiter chamber, the behavior of the neutral particles is calculated by the two-dimensional Monte-Carlo code.

2.1 Recycling model of neutral particles

Details of the recycling model of neutral particles at various points on the limiter and wall in the one-dimensional tokamak transport code are as follows.

Neutral particles colliding with the limiter and wall are assumed to be reflected at the rate given by

$$R_N(E_{in}, \theta) = 1 + (1 - \frac{\theta}{90°})(R_N^0(E_{in}) - 1) \quad , \tag{2-1}$$

$$R_N^0(E_{in}) = -0.24 \log_{10}(\frac{E_{in}}{E_L}) + 0.19 \tag{2-2}$$

and with the energy given by

$$E_{ref} = \frac{R_E(E_{in}, \theta)}{R_N(E_{in}, \theta)} E_{in} \quad , \tag{2-3}$$

$$R_E(E_{in}, \theta) = 1 + (1 - \frac{\theta}{90°})(R_E^0(E_{in}) - 1) \quad , \tag{2-4}$$

$$R_E^0(E_{in}) = -0.22 \log_{10}(\frac{E_{in}}{E_L}) + 0.06 \quad , \tag{2-5}$$

$$E_L = \begin{array}{ll} 2990 & \text{for D,T} \\ 6290 & \text{for He} \end{array} \quad , \tag{2-6}$$

where E_{in} is the incident energy, E_{ref} the reflection energy and E_L the reduced energy factor given in Ref. 9. There are few experiments and theories concerning the reflection coefficients R_N and R_E, except for the normal incidence [11]. Only the numerical calculation shows that the reflection coefficients approaches to unity as θ goes to 90°[12]. Therefore we assume for simplicity the linear angular dependence in Eqs. (2-1) and (2-2). Other particles that are not reflected are adsorbed and then desorbed at wall temperature. The angle of reflected or desorbed particles is assumed to be isotropic. Deuterium and tritium particles desorbed from the limiter and wall or gas-puffed are of molecular form. These molecules will soon be dessociated, so that we assume the energy of fuel particles desorbed or gas-puffed to be 5 eV (Frank-Condon neutral energy). Since the diffused ion particles

and charge-exchange neutral particles will collide with the fisrt wall or limiter isotropically, we use the averaged value of R_i and R_E with respect to θ (i.e., $\theta = 45°$). Ion flux to the limiter along the magnetic field line is accelerated by the sheath potential, so that $E_{in} = T_i + 3Z\ T_e$ (where T_e, T_i and Z are electron and ion temperature and charge of the ion) and $\theta = 0°$ are used. Recycling rate at each point on the first wall and limiter is unity. Thus, the total number of neutrals reentering into the plasma from these points is equal to the sum of the ions and charge-exchange neutrals entering into these respective points.

The average energy of neutral particles, which flow back to the main plasma from the pumped limiter chamber is calculated by the two-dimensional Monte-Carlo neutral code. This code is the improved one, original of which was developed to calculate the helium ash exhaust [4]. Details of the code are presented in Ref. 13, so that we will review briefly only the essential points as follows.

The neutral particle motions initiated at the neutralizer plate are followed by the improved Monte-Carlo simulation method with fixed plasma parameters of the scrape-off layer in the limiter chamber. The particle trajectories were tracked at a fixed time interval in Ref. 4, while in the present model they are improved to be traced at a space interval between space lattices. It allows the neutral distributions to be easily calculated. Neutral particles traversing the scrape-off plasma have chances for ionization and charge exchange reactions with plasmas. The reaction points are searched within the space interval by generating a random number according to the reaction probability.

After ionization of neutral particles, the newborn ions are

tracked from the reaction point, while after the charge exchange a new velocity is assigned to the neutral particle by generating a random number according to the Maxwell velocity distribution of the background ions. A new velocity is also given to a reflected neutral in collision with the limiter chamber wall, which is given by Eqs. (2-1) ∿ (2-6).

The tracking of neutral particles is terminated when they return back to the main plasma region across the entrance of limiter chamber, or leave the entrance of the evacuating duct. On the other hand, ions are traced until they reach the neutralizer plate again, or until leaving the entrance of limiter chamber, or until flowing out of the scrape-off layer to the chamber wall by diffusion perpendicular to magnetic field line.

The ionization process of neutral atoms is described on the basis of the ionization rate coefficients by the Freeman and Jones formula[14] for fuel particles and Lotz's formula[15] for heliums. As for the charge exchange, the Riviere's formula[16] is used.

The average energies of fuel and helium neutral particles, which flow back to the main plasma, are calculated by this code over the wide range of parameters of the scrape-off layer plasma. The results are shown in Fig. 2. In the case of fuel particles, since the major fraction of the neutrals flowing back to the main plasma have experienced charge exchange reactions, the average energies are almost the same as that of scrape-off plasma. While, the charge exchange reaction can be neglected for helium, so that they loose their energy monotonically by the collision with the wall and the energy becomes lower than that of the scrape-off plasma as shown in the figure. These results are not so affected by the density of the scrape-off plasma that we will neglect

their density dependence, for simplicity.

The backflow fraction R_s can also be calculated by this code as a function of the effective pumping speed C_d at the entrance of the evacuating duct. The backflow fraction is defined as the ratio of the particle flow flowing back to the main plasma to that flowing into the limiter chamber. This value strongly depends on the density of the scrape-off plasma, while is little affected by the temperature. The results are shown in Fig. 3 with the density as a parameter.

The values of R_s for deuterium, tritium and helium differ slightly to each other depending on the processes of the neutral-wall interaction adopted [4, 17]. In the present paper, we will assume for simplicity that R_s takes the same value for D, T and He. This assumption becomes correct when the density of the scrape-off plasma becomes high [4, 17]. The effect of the opening width of the limiter chamber is rather small, if the length of the chamber is longer than 40 $\sim$ 50 cm[4], so that we also assume that R_s is not affected by the limiter length. It should be noted that the effective pumping speed C_d of the abscissa is defined at the entrance of the evacuating duct. The pumping speed for fuel particles at the very front of the pump, especially for cryo-pump, is fairly larger than that for helium. While, the conductances of the evacuating duct for fuel particles (D_2, DT, T_2) are smaller than that for helium by a factor of the square root of mass ratio, so that the former differences will strongly be compensated by the latter. Therefore, it will be reasonable to assume that R_s of fuels and helium take the same value for the same pumping capacity.

2.2 Model of one-dimensional transport code

(1) Neutral particle density in the main plasma including the scrape-off layer is calculated by solving the Boltzmann neutral transport equation in cylindrical geometry [18]. This equation can be transformed to the following integral equation for the neutral density N(r) and can be solved by iteration method.

$$N(r) = \int_r N(r')\,\tilde{\psi}(r, r')\,dr' + \psi(r) \quad . \tag{2-7}$$

The second term on the R.H.S. represents the parents generation which is the density of the first generation neutral particles entering into the plasma from the limiter or wall. The first term is the child generation which is generated by charge exchange reaction. For helium particles, only the second term is retained, since we neglect the charge exchange process. The expression for the parents generation $\psi(r)$ is

$$\psi(r) = \sum_{i}^{N_{mesh}} \sum_{j}^{N_{energy}} N_0^j \exp\left[-\int_r^{r^i_{max}} \beta(\xi)\tau(r, \xi)d\xi\right]. \tag{2-8}$$

where $$\beta = (n_e\,\alpha_{ei} + n_i\,\alpha_{ii} + n_i\,\alpha_{cx})/v_0^j \quad . \tag{2-9}$$

Here n_e, n_i, α_{ei}, α_{ii}, α_{cx} are electron and ion density, the rate coefficients for electron and ion impact ionization and charge exchange reaction, respectively. The term τ represents the geometrical factor for cylindrical coordinate system. The neutral density N_0^j with velocity v_0^j at each generation point on the limiter and wall, r^i_{max} is given from the total particle flux to that point according to the recycling model. By summing up all of the parents generations with various N_0^j, v_0^j and r^i_{max} (total number is

$N_{mesh} \times N_{energy}$, where N_{mesh} is the total number of mesh on limiter and wall, N_{energy} is the total number of energy group), the total neutral density by parents generation is obtained. The total neutral density N(r) can be obtained by successive iteration of Eq. (2-7) or by multiplying $\psi(r)$ by the operator $(I - \int \tilde{\psi}(r,r')dr')^{-1}$ in the differenced form of Eq. (2-7), where I is a unit matrix.

(2) Transport model in the main plasma

We use the standard INTOR scaling for the transport in the main plasma as follows [19].

$$\chi_e \text{(electron thermal conductivity)} = \frac{5 \times 10^{19}}{n_e(r)} \quad , \tag{2-10}$$

$$\chi_i \text{(ion thermal conductivity)} = 3\,\chi_{neocl.} \quad , \tag{2-11}$$

$$D \text{ (particle diffusion coefficient)} = \frac{\chi_e}{5} \quad , \tag{2-12}$$

where $\chi_{neocl.}$ is the neoclassical ion conductivity. Since the typical operation parameter of the plasma ($\bar{T}_i \sim 10$ keV, $\bar{n}_i \sim 1.4 \times 10^{20}$ m^{-3}) is thermally unstable for this transport model, the equilibrium state is obtained by calculating the time evolution (50 ~ 60 seconds) with the appropriate feedback control of the plasma temperature and density [20, 21].

(3) Transport model in the scrape-off layer

Particle and electron and ion energy losses along the magnetic field line are

$$\frac{n}{\tau_{//}} \qquad \text{for particle} \quad , \tag{2-13}$$

$$\gamma_e \frac{n_e T_e}{\tau_{//}} \qquad \text{for electron, energy} \quad , \tag{2-14}$$

$$\gamma_i \frac{n_i T_i}{\tau_{//}} \qquad \text{for ion energy} \quad , \tag{2-15}$$

$$\tau_{//} = \frac{L}{v_f} \quad , \tag{2-16}$$

where $\tau_{//}$, γ_e and γ_i are the life time of the particle along the magnetic field line with the length of L, electron and ion heat transmission coefficients, respectively. We use the typical values of $\gamma_e = 5.8$ and $\gamma_i = 2.0$ according to the simple sheath theory [22]. We also use the typical value of the flow velocity v_f; $v_f = 0.3\ C_s$ (C_s is the ion sound velocity) [23].

Transport coefficients in radial direction are of Bohm type and are assumed constant through the scrape-off layer as follows,

$$D = \chi_e = \chi_i = C_B\, D_{Bohm}(r_s) \quad , \tag{2-17}$$

where $D_{Bohm}(r_s)$ is the Bohm diffusion coefficient determined at the separatrix line r_s. We use the typical value of 0.3 for the ambiguity factor C_B [23].

(4) Fueling model

We employ two methods for fueling; pellet injection and gas-puffing. We use the simplified penetration model for the pellet injection [24]. The particle source profile by pellet is linearly decreasing from the plasma surface and the penetration depth ℓ is determined by the following equation.

$$U\, r_p^{5/3} = \frac{2.92 \times 10^{-6} a}{M^{1/3}} \int_{1-\ell/a}^{1} L(T_e/2)^{1/3}\, n_e^{1/3}\, T_e^{1/6} \tag{2-18}$$

$$\times \left\{ T_e + 8.5 \times 10^{-4}\, T_e^{\,2} - \frac{850}{T_e} + 75 \right\} d(r/a) \quad ,$$

where U, r_p and M are the injection velocity, radius and mass number of the pellet. $L(T_e/2)$ is a simple algebraic function of T_e given in Ref. 24.

In gas-puffing case, neutral particles enter into the main plasma from the wall with Frank-Condon energy of 5 eV. We consider the following three fueling scenarios as typical references.

pelle ① r_p = 1 mm ; U = 2×10^3 m/s (shallow penetration) .

pellt ② r_p = 3 mm , U = 10^4 m/s (moderate penetration) .

gas-puffing 5 eV neutral energy (surface fueling) .

The case of pellet ① , which will be realistic by the present-day technology, gives shallow penetration (∿ 30 cm) for the present plasma parameters. Even in the case of pellet ② , which may require enormous effort of development to realize, only moderate penetration (∿ 50 cm) is attained.

(5) Other energy terms

Total α-heating is 80∿85 MW for all cases. Bremsstrahlung and synchrotron radiation, ionization and charge exchange energy losses are taken into account. Total power of 50 ∿ 55 MW is carried by charged particles through scrape-off layer to the pumped limiter.

(6) Device parameters

As a reference reactor, we will employ the INTOR parameters as follows [19].

a	(plasma minor radius)	1.2 m
R	(plasma major radius)	5.3 m

B_t (toroidal field at axis)	5.4 T
I_p (plasma current)	6.4 MA
$\bar{T}_i$ (average ion temperature)	10 keV
$\bar{n}_i$ (average ion density)	1.4×10^{20} m^{-3}

3. Results of Calculations

3.1 Parameters of scrape-off layer plasma

First of all, various plasma parameters of the scrape-off layer are calculated for the typical case. These results are important for helium ash exhaust, heat load and erosion of the limiter. Pellet injection ① is used for the fueling as a reference. This pellet parameter is the typical value, which is expected to be realized by the present-day technology [25]. The width of the scrape-off layer is assumed to be 10 cm at the midplane. We define the separatrix line as the boundary magnetic field line, which separates the main plasma and scrape-off layer plasma (in contrast to the usual separatrix line, any null point does not appear on it in the present definition). We also define the limiter length ℓ_L, which is the distance between the leading edge of the limiter and the separatrix line projected to the minor radius direction as shown in Fig. 1. We choose three cases ℓ_L = 3, 5 and 7 cm as typical cases. For the backflow fraction, we choose R_s = 0.8, since, as is shown later, this value is sufficient and necessary to exhaust the helium ash by the realistic pumping speed.

Figures 4 and 5 show the electron temperature and density in the scrape-off layer. The arrows on the figures indicate the position of the leading edge of the limiter. As ℓ_L becomes longer, particle recycling

B_t (toroidal field at axis)	5.4 T
I_p (plasma current)	6.4 MA
$\bar{T}_i$ (average ion temperature)	10 keV
$\bar{n}_i$ (average ion density)	1.4×10^{20} m^{-3}

3. Results of Calculations

3.1 Parameters of scrape-off layer plasma

First of all, various plasma parameters of the scrape-off layer are calculated for the typical case. These results are important for helium ash exhaust, heat load and erosion of the limiter. Pellet injection ① is used for the fueling as a reference. This pellet parameter is the typical value, which is expected to be realized by the present-day technology [25]. The width of the scrape-off layer is assumed to be 10 cm at the midplane. We define the separatrix line as the boundary magnetic field line, which separates the main plasma and scrape-off layer plasma (in contrast to the usual separatrix line, any null point does not appear on it in the present definition). We also define the limiter length ℓ_L, which is the distance between the leading edge of the limiter and the separatrix line projected to the minor radius direction as shown in Fig. 1. We choose three cases ℓ_L = 3, 5 and 7 cm as typical cases. For the backflow fraction, we choose R_s = 0.8, since, as is shown later, this value is sufficient and necessary to exhaust the helium ash by the realistic pumping speed.

Figures 4 and 5 show the electron temperature and density in the scrape-off layer. The arrows on the figures indicate the position of the leading edge of the limiter. As ℓ_L becomes longer, particle recycling

increases, so that the temperature decreases and the density increases. The characteristic decay length of the temperature is considerably short ($\sim$ 2 cm), while that of density is fairly long (not the exponential type). This feature makes the helium ash exhaut rather easier.

Figures 6 and 7 show the fuel and helium particle flux in poloidal direction in the scrape-off layer. Reflecting the broad density profile, their decay lengthes are considerably longer than that of temperature. The dependence of helium particle flux on ℓ_L is much stronger than that of fuel particles. This is because the helium particle recycling becomes much smaller when large fraction of the particles ($1 - R_s = 0.2$) are pumped out by decreasing ℓ_L, while fuel particle recycling cannot become so small, since fuel particles pumped out must be supplied to keep the density of fuels constant. Figure 8 shows the total heat flux Q in poloidal direction in the scrape-off layer. Since $Q \propto nT^{3/2}$ and n and T have the inverse dependence on ℓ_L, Q has little dependence on ℓ_L. The characteristic decay length is shorter than that of temperature by a factor of 1.5, which arises from the T dependence of Q.

3.2 Helium ash accumulation and exhaust

In the next place, we investigate the helium ash accumulation and exhaust in detail. Figure 9 shows the helium ash accumulation in the main plasma as R_s is varied for ℓ_L = 3, 5 and 7 cm. Fueling is performed by pellet injection ①. If the allowable accumulation is 5%, for instance, the required backflow fractions R_s are 0.96 (ℓ_L = 3 cm), 0.91 (5 cm) and 0.74 (7cm), respectively. When the values of R_s become larger than these required values, the accumulation becomes large very rapidly. While, when the values of R_s are decreased, the accumulation decreases only

slightly. Even if all of the particles entering into the limiter chamber are exhausted ($R_s = 0$), the accumulation remains at about 4%. Note, however, that in the case of ℓ_L = 5 cm for example, only about 20% of the recycling helium particles flow into the limiter chamber and the rest of the particles recycle on the limiter surface as can be seen from Fig. 7. Thus, the recycling rate for the whole helium particles reduces down to 0.8 at most, even though R_s approaches to zero. Considering that the saturated helium accumulation of 4% does not change for various ℓ_L and over the wide range of R_s, this value should be determined by the particle balance between the helium particle confinement time in the central region of the plasma (we call it the bulk plasma later on) and the production rate of α-particles. This fact also implies that the helium confinement time in the bulk plasma is not affected by the helium particle recycling in the boundary plasma untill the value of R_s becomes large (around the requried values mentioned above) or the accumulation becomes about 5%. Thus, the allowable helium accumulation of 5% is fairly reasonable from the view point of cost-performance. As a matter of course, this reasonable value of allowable helium accumulation varies with the fusion power density of the reactor. The value becomes large, when the fusion power density becomes large.

We now evaluate the pumping speed to realize the required backflow fractions. To do so, the average densities of the limiter chamber (the average density of the scrape-off layer, which covers the opening of the limiter chamber) are shown in Fig. 10 for each ℓ_L as R_s is varied. On the same figure, the relations between the plasma density and R_s of Fig. 3 with C_d being constant are also shown by long broken lines. From this figure, we see that the required pumping speed C_d is 5×10^4 ℓ/s to realize $R_s = 0.74$ for ℓ_L = 7 cm. This is rather small

pumping speed. If we assume that 5×10^5 ℓ/s is around the limiting value of the reactor engineering, fairly small value of R_s (0.2 ∿ 0.3) can be realized for all of ℓ_L. Furthermore, in the limiter chamber, the plasma density may be expected very high due to the high recycling of the particle as in the divertor chamber [26, 27], as a result of which the requried pumping speed could be further reduced. For these reasons, we can consider rather wide range of operation regimes for the pumped limiter (i.e. operation regime of high pumping with high edge plasma temperature and that of low pumping with medium edge plasma temperature).

Let us now evaluate the particle load to the pump. Figure 11 shows the overall particle confinement times of D, T and He for ℓ_L = 5 cm. In the case of the helium particles, the overall particle confinement time τ_{He} becomes longer and approaches to that in the bulk plasma, as the pumping speed becomes large. Note, however, that the helium confinement time in the bulk plasma obtained by the saturated accumulation (4%) of Fig. 9 is about 5 seconds, so that τ_{He} in Fig. 11 even for R_s = 0 is still smaller than that in the bulk plasma by an order of magnitude. This implies that the recycling rate for the whole helium particles is still large even when R_s approaches to zero. This is the reason why the helium accumulation in Fig. 9 saturates as R_s becomes small, while τ_{He} increases monotonically in Fig.11. In the case of fuel particles, pumped out fuels must be supplied by pellet injection to keep the fuel density constant. By the present typical values of pellet size and speed, it is difficult to penetrate so deeply into the plasma, that the overall particle confinement time τ_D, τ_T cannot be such long as τ_{He}. τ_{He} is always longer than τ_D and τ_T, except for R_s, which is very near to unity. It should be born in mind that the behaviors of helium and

hydrogen of the reactor plasma differ in this way from those of the conventional plasma. This fact implies that more fuel particles will be pumped out. To investigate this, we define the helium enrichment factor f_e as

$$f_e = \frac{\Gamma_{He}^P / \Gamma_i^P}{\bar{n}_{He} / \bar{n}_i} \quad ,$$

where Γ_{He}^P, Γ_i^P, $\bar{n}_{He}$ and $\bar{n}_i$ are the particle flux being pumped out and the average density in the main plasma for helium and fuel ions, respectively. Figure 12 shows f_e as R_s is varied for various ℓ_L. Helium particles are enriched when $f_e > 1.0$, and anti-enriched when $f_e < 1.0$. When R_s is smaller or ℓ_L is shorter, helium is expected to be strongly anti-enriched. This tendency is qualitatively consistent with the present-day experiments of helium ash exhaust [28]. As is mentioned in Fig. 9, the helium confinement time in the bulk plasma begins to be affected by the helium recycling in the boundary when the accumulation is about 5%. Around the corresponding values of R_s, τ_{He} begins to become shorter than τ_D and τ_T, so that f_e becomes unity around these values of R_s.

In practice, the absolute amount of tritium pumped out is more important than the characteristics of helium enrichment for the particle load to the pump or the required amount of circulating tritium. The results are shown in Fig. 13. The amount of tritium pumped out becomes smaller when R_s is larger and/or ℓ_L is longer. If, however, we intend to realize the same heluim accumulation (5%) by different values of ℓ_L, the absolute amounts of tritium pumped out are almost the same for all ℓ_L as shown by the arrows in the figure. When the allowable helium accumulation can be increased, the amount of tritium pumped out can be

decreased. This can be an important factor for the optimization of the pumped limiter.

3.3 Heat load and erosion

In considering the heat load and erosion of the limiter, the electron temperature and density of the scrape-off plasma and the total ion particle flux to the limiter and chamber are important parameters. Figures 14, 15 and 16 show the electron temperature at the separatrix, the average electron density of the scrape-off plasma and the total ion particle flux to the limiter and chamber, respectively, as R_s is varied for various ℓ_L. Fueling is performed by pellet injection ①. The arrows on the figures show the corresponding values of temperature, density and flux to keep the helium accumulation in the main plasma at 5%. The differences of these coresponding values for each ℓ_L are fairly small, that is, $T_{es} = 430 \sim 450$ eV, $\bar{n}_{es} = 1.9 \sim 2.3 \times 19^{19}$ m^{-3} and $\Gamma_i = 2.4 \sim 2.8 \times 10^{22}$ s^{-1}. These values of temperature and ion particle flux may not be preferable, since the erosion rate may take its maximum value. To avoid the maximum erosion, the plasma temperature T_{es} should be lowered or raised. T_{es} could be lowered by increasing R_s, while, in this case, the helium accumulation in the main plasma becomes high as shown in Fig. 9. Although this operation regime of low T_{es} is very attractive since the erosion rate can be lowered, the amount of tritium pumped out can be reduced and the required pumping speed can be decreased, we cannot employ this operation regime unless the restriction of the helium accumulation in the main plasma is relaxed. In the case of the operation regime of high T_{es}, the erosion rate could be lowered, since the total ion particle flux Γ_i is reduced. As shown in Fig. 14,

T_{es} can be raised by decreasing R_s and ℓ_L. However, T_{es} can be raised at most up to about 500 eV even when $R_s < 0.5$. If we consider pellet injection ② , which seems more ideal than ① , higher T_{es} can be realized. Figures 17 and 18 show T_{es} and Γ_i by various fueling methods for ℓ_L = 3 cm (pellet ① and ② and gas-puffing) and ℓ_L = 5 cm (pellet ②) as R_s is varied. There is no appreciable difference between pellet injection ① and gas-puffing. In the case of pellet injection ② , the overall particle confinement time becomes considerably long and the density of the scrape-off layer plasma becomes low, so that $R_s \sim 0.5$ will be the lowest value available by the limiting pumping speed of 5×10^5 ℓ/s as shown in Fig. 19. T_{es} can be raised up to 700 ∿ 900 eV, when $R_s = 0.5$.

Let us now evaluate the heat load and erosion of the limiter for the case of medium T_{es} (Case I; pellet injection ① , $R_s = 0.8$, $\ell_L = 7$ cm, $T_{es} = 420$ eV) and for the case of high T_{es} (Case II and III; pellet injection ② , $R_s = 0.5$, $\ell_L = 3$ cm and 5 cm, respectively). Since the heat load and erosion depend strongly on the position and configuration of the limiter, they should be evaluated in the practical design. We will install the limiter at the bottom of the plasma and use the equilibrium magnetic field configuration according to the INTOR design [25]. The heat and ion particle flux, ion and electron temperature on the midplane calculated so far by the one-dimensional transport code are projected on the limiter surface along the equilibrium magnetic field line. Figures 20 and 21 show the distributions of the heat and ion flux and erosion on the limiter surface for Case I and III, respectively. In evaluating the erosion, we assume that the material of the limiter is carbon, of which physical sputtering coefficiemt is determined by Smith's formula [29], and chemical sputtering coefficient by the experimental one [30] with the temperature of the limiter surface being assumed 500°C.

We also assume that the duty cycle is 80% and the availability is 50%. As for the self-sputtering, we assume that average charge state and the concentration of the carbon is 3 and 2% and neglect the redeposition. As can be seen from these figures, the heat and ion flux and the erosion on the large-major-radius side limiter are larger than those on the small-major-radius side limiter due to the toroidal shift of the plasma. The erosion rate of Case III is reduced by a factor of two at the maximum than that of Case I.

The heat and ion flux and the erosion both at the maximum point and the leading edge of the limiter are summarized in Table 2 for Case I ∿ III. Since the chemical sputtering is dominant for the erosion of carbon, we also tabulated the erosion of iron as a reference, which is dominated by the physical sputtering. In evaluating the erosion of iron by self-sputtering, we assume taht the average charge state and the concentration of iron are 3 and 0.5%. Quantitative tendency of the erosion both of carbon and iron is almost the same. From this table, we see that the erosion at the maximum is reduced by a factor of two or more by realizing the operation regime of high T_{es}, while the heat flux is almost the same for Case I ∿ III. In the case of Case II, however, the heat flux on the leading edge is quite large and may exceed the limiting value of the reactor engineering. The erosion is also very large. To lower these values, it is necessary to install the limiter with longer ℓ_L. In the case of Case III, the heat flux on the leading edge is decreased significantly, while the erosion is still rather large. When the length of the limiter is further lengthened, the particle recycling on the limiter surface dominates the overall particle recycling, so that the difference by the pumping and fueling scheme between Case I and Case II, III almost vanishes. To determine the best operation regime, it is necessary to consider the detailed

design carefully, since the engineering limitation of the heat flux and erosion strongly depends on the practical design. The operation regime of Case II seems unrealistic, since the heat flux to the leading edge is too large. The operation regime of Case III is preferable in the erosion at the maximum point, while that of Case I can be more preferable since the heat flux and erosion of the leading edge tend to be the most critical engineering limitation. It should also be noted that, in Case III, the amount of tritium pumped out is much larger than that in Case I and that the development of the technology of pellet injection ② will require enormous effort. On the basis of the above considerations, the best configuration and operation regime of the pumped limiter for INTOR at present will be summarized as follows.

Limiter length on the midplane:	7 cm,
Effective pumping speed at duct entrance:	5×10^4 ℓ/s ,
Fueling:	pellet injection ① ,
Electron temperature at separatrix:	about 400 eV .

4. Engineering Considerations for the Pumped Limiter

4.1 Mechanical configuration and operating conditions.

The main purpose of this section is to develop a feasible limiter design. The double-null poloidal divertor concept is selected as a reference for FER. A single-null poloidal divertor and a single pumped limiter are proposed as alternative options. The same major plasma parameters as in the double-null divertor solution are considered for the alternative solutions.

The limiter operating conditons are given in Table 3. The maximum heat flux on the top surface is 2 MW/m^2 and that on the leading edge is

design carefully, since the engineering limitation of the heat flux and erosion strongly depends on the practical design. The operation regime of Case II seems unrealistic, since the heat flux to the leading edge is too large. The operation regime of Case III is preferable in the erosion at the maximum point, while that of Case I can be more preferable since the heat flux and erosion of the leading edge tend to be the most critical engineering limitation. It should also be noted that, in Case III, the amount of tritium pumped out is much larger than that in Case I and that the development of the technology of pellet injection ② will require enormous effort. On the basis of the above considerations, the best configuration and operation regime of the pumped limiter for INTOR at present will be summarized as follows.

Limiter length on the midplane:	7 cm,
Effective pumping speed at duct entrance:	5×10^4 ℓ/s ,
Fueling:	pellet injection ① ,
Electron temperature at separatrix:	about 400 eV .

4. Engineering Considerations for the Pumped Limiter

4.1 Mechanical configuration and operating conditions.

The main purpose of this section is to develop a feasible limiter design. The double-null poloidal divertor concept is selected as a reference for FER. A single-null poloidal divertor and a single pumped limiter are proposed as alternative options. The same major plasma parameters as in the double-null divertor solution are considered for the alternative solutions.

The limiter operating conditons are given in Table 3. The maximum heat flux on the top surface is 2 MW/m^2 and that on the leading edge is

0.35 MW/m^2. The maximum particle flux on the top surface is $1.1\times10^{22}/s\text{-}m^2$ and the electron temperature there is 150 eV. The maximum particle flux and the electron temperature on the leading edge are $7.3\times10^{21}/s\text{-}m^2$ and 44 eV. During the plasma disruption, the peak energy flux at the limiter plate is 270 J/cm^2 during the 5-ms thermal quench.

The limiter plate is installed at the bottom of the reactor core as shown in Fig. 22. The flat, double-edged limiter is considered. The limiter consists of 28 sectors, 2 sectors between two TF coils. Each sector is retracted horizontally by single straight motion for the limiter replacement. The limiter plate is composed of surface armor tiles, cooling plates and structure reinforcements. The armor tiles are brazed to the cooling plates. Candidate materials considered for the armor tiles are graphite, pyrolitic graphite, silicon carbide and beryllium. The materials for the cooling plate and the structure reinforcement are 0.2% Ag OFCu and type 316 stainless steel.

4.2 Thermal hydraulics and stress analysis

Several armor materials - C, PG, SiC and Be have been considered in the thermal hydraulics and stress analysis. The armor material thickness is varied from 5-mm to 20-mm in the analysis. The cooling plate thickness is constant at 2-mm. The thermal conductivities of armor materials may decrease under irradiation. The thermal conductivities under irradiation are assumed to be 30 W/m-k for C and PG, and to be 20 W/m-k for SiC in the analysis. Two different geometries are used for the top surface and the leading edge analysis. The top surface is calculated by a two-dimensional plane model, and the leading edge is calculated by a two-dimensional axisymmetric model.

Table 4 and Table 5 show the temperature and thermal stress of the

limiter with 10-mm thick tile at the top surface and the leading edge, respectively. The maximum allowable temperatures for the tile materials are determined by vaporization loss and chemical sputtering. The temperature and thermal stress at the leading edge with the heat flux of 0.35 MW/m^2 are lower than those at the top surface with the heat flux of 2 MW/m^2. In the unirradiated condition, the maximum temperatures of all tiles at the top surface are near or below the allowable temperatures. However, the maximum temperatures of the C and PG tiles at the top surface after irradiation are over the allowable ones. Results of the stress analysis indicate that the SiC tile limiter at the top surface and the PG tile limiter do not satisfy the limit of stress intensity.

4.3 Reference design selection

Table 6 and Table 7 show the allowable thickness and lifetime of tiles at the top surface and the leading edge of limiter, respectively. The allowable thickness is determined by the maximum allowable temperature and allowable stress. The erosions considered for tile materials are the loss during plasma disruption and the physical sputtering. The erosion by disruption is the total of vaporized and melt layers assuming melt layer is lost. The chemical sputtering of graphite is neglected because the maximum allowable temperature of graphite is 400°C and without the severe range of the sputtering.

The lifetime at the leading edge is always longer than that at the top surface. Graphite has the longest lifetime in the unirradiated condition, and the lifetime of 0.6 year after irradiation. The lifetime of beryllium is 0.9 year. Pyrolitic graphite and silicon carbide have the short lifetime because of the thin thickness due to stress limit. The limiter plate of the graphite tiles is selected as the reference limiter.

The study of the thermal conductivity under irradiation is the subject for a future R&D. The alternative tile material is beryllium.

4.4 Analysis for alternative operating conditions

The physical considerations for the pumped limiter show that there are other operating conditions of the limiter as summarized in Table 2. To clarify the engineering limitation on the operating conditions, we have done the analysis for another conditions. The alternative operating conditions are given in Table 8. The maximum heat flux on the top surface is 3 MW/m^2 and that on the leading edge is 1 MW/m^2.

The temperature and thermal stress of the limiter with 10 mm thick tile are shown in Table 9 and Table 10 for the top surface and the leading edge, respectively. Table 11 shows the allowable thickness and lifetime at the top surface and Table 12 shows the ones at the leading edge. For the graphite tile limiter, the lifetime at the top surface is shorter than that at the leading edge. At the top surface, the graphite tile limiter with the heat flux of 3 MW/m^2 has shorter lifetime by a factor of two than that with the heat flux of 2 MW/m^2. The lifetime of graphite tile at the leading edge with the heat flux of 1 MW/m^2 is almost the same as that at the top surface with the heat flux of 2 MW/m^2.

5. Conclusions

We developed a detailed recycling model of neutral particles on the limiter and first wall in the one-dimensional tokamak transport code, and incorporated the energy of neutrals, which flow back from the limiter chamber, calculated by the two-dimensional Monte-Carlo neutral code. The optimum configuration and operation regime of the pumped limiter in INTOR were analysed. The main conclusions obtained

The study of the thermal conductivity under irradiation is the subject for a future R&D. The alternative tile material is beryllium.

4.4 Analysis for alternative operating conditions

The physical considerations for the pumped limiter show that there are other operating conditions of the limiter as summarized in Table 2. To clarify the engineering limitation on the operating conditions, we have done the analysis for another conditions. The alternative operating conditions are given in Table 8. The maximum heat flux on the top surface is 3 MW/m^2 and that on the leading edge is 1 MW/m^2.

The temperature and thermal stress of the limiter with 10 mm thick tile are shown in Table 9 and Table 10 for the top surface and the leading edge, respectively. Table 11 shows the allowable thickness and lifetime at the top surface and Table 12 shows the ones at the leading edge. For the graphite tile limiter, the lifetime at the top surface is shorter than that at the leading edge. At the top surface, the graphite tile limiter with the heat flux of 3 MW/m^2 has shorter lifetime by a factor of two than that with the heat flux of 2 MW/m^2. The lifetime of graphite tile at the leading edge with the heat flux of 1 MW/m^2 is almost the same as that at the top surface with the heat flux of 2 MW/m^2.

5. Conclusions

We developed a detailed recycling model of neutral particles on the limiter and first wall in the one-dimensional tokamak transport code, and incorporated the energy of neutrals, which flow back from the limiter chamber, calculated by the two-dimensional Monte-Carlo neutral code. The optimum configuration and operation regime of the pumped limiter in INTOR were analysed. The main conclusions obtained

are summarized as follows.

(1) The electon temperature in the scrape-off layer decays rather rapidly with the characteristic decay length of about 2 cm, while the density distribution is fairly broad.

(2) Even when a considerably long limiter is installed (e.g. 7 cm on the midplane), not so large pumping speed is sufficient to keep the helium accumulation in the main plasma at the desired level (e.g. 5×10^4 ℓ/s for 5% in INTOR). There is a certain pumping speed, above which the accumulation of the helium in the main plasma decreases only slightly even when the pumping speed is increased, while, under which, it increases very rapidly as the pumping speed is decreased.

(3) Overall particle confinement time for helium becomes much longer than that for fuel particles, when more particles are pumped out by larger pumping speed, and the helium particles tend to be anti-enriched.

(4) The minimum amount of tritium pumped out is almost uniquely determined by the allowable helium accumulation in the main plasma. This value little depends on the length of the limiter, if the pumping speed is appropriately adjusted so as to keep the accumulation at the same level. It is smaller as the allowable accumulation level is higher.

(5) The electron temperature at the boundary is 400∿500 eV when the realistic pellet injection by the present-day technology is employed. It will be difficult to further lower the temperature without increasing the helium accumulation level. Fueling by gas-puffing gives almost the same resutls.

(6) The high temperature operation regime (700∿900 eV) could be realized

by large pumping and ideal pellet injection with short limiter length, and the maximum erosion on the limiter surface could be decreased by a factor of two or more. However, if the heat flux and eorsion of the leading edge are more critical for the engineering, the high temperature operation regime is not necessarily preferable:

On the basis of these results, the best configuration and operation regime of the pumped limiter at present will be as follows. Limiter length on the midplane is 7 cm, effective pumping speed at evacuating duct entrance is 5×10^4 ℓ/s, fueling is performed by pellet injection ① and electron temperature at separatrix is about 400 eV (medium temperature operation regime).

One of the effects, which is neglected in the present calculation, is the compatibility between the pumped limiter and the hot core plasma. For instance, in Case I in Table 2, the maximum erosion of 16 cm for carbon implies that a considerable amount of carbon will enter into the main plasma as impurities. As a result, the boundary plasma will be cooled to a certain extent and the main plasma may somewhat be affected. This investigation requires the detailed analysis of the impurity transport, and is beyond the scope of the present study. Major modifications by this effect to the calculations of the present study will be expected as follows. The absolute value of the heat flux and erosion may be decreased, while the relative value and the qualitative features will not be changed so much.

The effect of the increase of the particle recycling in the limiter chamber is also neglected in the present study. It will significantly affect the relation between the pumping speed and the backflow fraction. The required pumping speed will be further decreased

by this effect. Since large fraction of the particles are recycling on the limiter surface, it will have no significant effect on the overall particle recycling, heat flux and erosion of the limiter in the present study. In the case of divertor, however, almost all of the particles flow into the divertor chamber, so that this effect becomes essential, especially in high density plasma [31 - 33]. In order to deal with this effect correctly, it is necessary to solve MHD equations along and perpendicular to the field line in the chamber consistently with the particle, momentum and energy source from the neutral particles [34 - 36]. This study is in progress and will be reported elsewhere in future.

Acknowledgements

We are grateful to Drs. M. Yoshikawa, K. Tomabechi, Y. Iso and S. Mori for their continuous encouragement.

by this effect. Since large fraction of the particles are recycling on the limiter surface, it will have no significant effect on the overall particle recycling, heat flux and erosion of the limiter in the present study. In the case of divertor, however, almost all of the particles flow into the divertor chamber, so that this effect becomes essential, especially in high density plasma [31 - 33]. In order to deal with this effect correctly, it is necessary to solve MHD equations along and perpendicular to the field line in the chamber consistently with the particle, momentum and energy source from the neutral particles [34 - 36]. This study is in progress and will be reported elsewhere in future.

Acknowledgements

We are grateful to Drs. M. Yoshikawa, K. Tomabechi, Y. Iso and S. Mori for their continuous encouragement.

References

[1] SHIMOMURA, Y., SAKO, K., SHINYA, K.: JAERI-M 8294 (1979).

[2] SENGOKU, S., AZUMI, M., MATSUMOTO, Y., MAEDA, H., SHIMOMURA, Y.: Nucl. Fusion 19 (1979) 1327.

[3] TAKIZUKA, T., AZUMI, M., SEKI, Y., SENGOKU, S., MAKI, K., et al.: in Plasma Physics and Controlled Nuclear Fusion Research (Proc. 8th Int. Conf. Brussels, 1980) Vol. 1, IAEA, Vienna 679 (1981).

[4] SEKI, Y., SHIMOMURA, Y., MAKI, K., AZUMI, M., TAKIZUKA, T.: Nucl. Fusion 20 (1980) 1213.

[5] INTOR GROUP: Nucl. Fusion 20 (1980) 349.

[6] SAKO, K., TONE, T., SEKI, Y., IIDA, H., et al.: JAERI-M 8518 (1979).

[7] NISHIO, S., SHIMADA, R., SHIMAMOTO, S., FUKAI, Y., SAWADA, Y., et al.: JAERI-M82-176 (1982).

[8] BAKER, C.C., ABDOU, M.A., et al., ANL/FPP-80-1 (1980).

[9] SAITO, S., FUJISAWA, N., SUGIHARA, M., UEDA, K., NAKAMURA, H., JAERI-M82-011 (1982).

[10] FUJISAWA, N., SUGIHARA, M., SAITO, S., SHIMADA, M., JAERI-M82-173 (1982).

[11] McCRACKEN, G.M., STOTT, P.E., Nucl. Fusion 19 (1979) 889.

[12] ONE, O.S., ROBINSON, M.T., J. Nucl. Mater. 76 & 77 (1970) 370.

[13] SAITO, S., SUGIHARA, M., FUJISAWA, N., ABE, T., UEDA, K., Nucl. Tech./Fusion (to be published).

[14] FREEMAN, R.L., JONES, E.M., CLM-R137, Culham Laboratory (1974).

[15] LOTZ, W., Z. Phys. 216 (1968) 241.

[16] RIVIERE, A.C., Nucl. Fusion 11 (1971) 363.

[17] CALLEN, J.D., EMMERT, G.A., BAILEY, A.M., BENCHIKH-LEHOCINE, M.E., DAVIDSON, J.N., et al., in Plasma Physics and Controlled Nuclear

Fusion Research (Proc. 8th Int. Conf. Brussels, 1980) Vol. 1, IAEA, Vienna (1981) 775.

[18] KOBAYASHI, T., TAZIMA, T., TANI, K., TAMURA, S., JAERI-M7014 (1977).

[19] INTOR GROUP, International Tokamak Reactor: Zero Phase (Rep. Int. Tokamak Reactor Workshop, Vienna, 1979), International Atomic Energy Agency, Vienna (1980).

[20] HOULBERG, W.A., ATTENBERGER, S.E., HIVELY, L.M., Nucl. Fusion 22 (1982) 935.

[21] HATAYAMA, A., SUGIHARA, M., HIRAYAMA, T., JAERI-M82-147 (1982).

[22] HOBBS, G.D., WESSON, J.A., Plasma Phys. 9 (1967) 85.

[23] DIVA GROUP, Nucl. Fusion 18 (1978) 1619.

[24] MIROLA, S.L., FOSTER, C.A., ORNL/TM-5776 (1977).

[25] INTOR GROUP, International Tokamak Reactor: Phase One (Rep. Int. Tokamak Reactor Workshop, Vienna, 1980-81), International Atomic Energy Agency, Vienna (192).

[26] OVERSKEI, D.O., Phys. Rev. Lett. 47 (1981) 177.

[27] SHIMADA, M., NAGAMI, M., IOKI, K., IZUMI, S., MAENO, M., et al., Nucl. Fusion 20 (1982) 643.

[28] SHIMADA, M., NAGAMI, M., IOKI, K., IZUMI, S., MAENO, M., et al., Phys. Rev. Lett. 47 (1981) 796.

[29] SMITH, D.L., J. Nucl. Mater. 75 (1978) 20.

[30] YAMADA, R., et al., J. Nucl. Mater, 95 (1980) 278.

[31] PETRAVIC, M., POST, D., HEIFETZ, D., SCHMIDT, J., Pys. Rev. Lett. 48 (1982) 326.

[32] SHIMADA, M., JAERI-M82-195 (1982).

[33] SHIMOMURA, Y., KEILHOCKER, M., LACKNER, K., MURMANN, H., SILLER, G., Max-Planck-Institute für Plasma physik Report, IPP III/80 (1982).

[34] HEIFETZ, D., POST, D., PETRAVIC, M., WEISHEIT, J., BATEMAN, G., J. Com. Phys. 46 (1982) 309.

[35] SHIMADA, M., NAGAMI, M., IOKI, K., IZUMI, S., MAENO, M., et al., J. Nucl. Mater. 111/112 (1982) 362.

[36] POST, D., HEIFETZ, D., PETRAVIC, M., ibid. p.383.

Table 1 Various requirements for pumped limiter and possible methods to meet them.

Requirement	Method
1. Helium exhaust	1. Position of leading edge
2. Pumped out tritium	2. Capacity of pump
3. Heat flux — Limiter surface, Leading edge	3. Fueling (pellet/gas-puff)
4. Erosion	

Table 2 Heat and ion particle flux, electron and ion temperature and erosion both at maximum point and leaing edge of limiter for Case I, II and III. Erosion is calculated both for carbon and iron limiter.

Case		Case I	Case II	Case III
		pellet ① $\ell_L = 7$ cm $R_s = 0.8$	pellet ② $\ell_L = 3$ cm $R_s = 0.5$	pellet ② $\ell_L = 5$ cm $R_s = 0.5$
maximum on limiter surface	heat flux (MW/m^2)	2.7	2.5	2.5
	ion flux ($1/m^2S$)	1.0×10^{22}	3.8×10^{21}	5.3×10^{21}
	electron temp. (eV)	150	410	220
	ion temp. (eV)	240	430	310
	erosion (cm/y) C	13.0	4.1	6.4
	erosion (cm/y) Fe	6.7	3.5	4.3
leading edge	heat flux (MW/m^2)	0.52	4.0	1.4
	ion flux ($1/m^2S$)	7.7×10^{21}	8.8×10^{21}	6.8×10^{21}
	electron temp. (eV)	44	360	130
	ion temp. (eV)	78	390	240
	erosion (cm/y) C	6.4	10	8.1
	erosion (cm/y) Fe	2.1	6.1	3.5

Table 3 Limiter operating conditions

Normal operation	
Total energy to limiter	40 MW
Ion flux	2.95×10^{23}/s
Edge electron temperature	280 eV
Composition of ions (average)	38%D, 55.5%T, 6%He, 0.5%Z
Peak heat flux normal to limiter surface	
Top surface (R=5.47m)	2 MW/m^2
Leading edge (R=5.78m)	0.35 MW/m^2
Peak ion flux normal to limiter surface	
Top surface (R=5.53m)	1.1×10^{22}/m^2-s
Leading edge (R=5.78m)	7.3×10^{21}/m^2-s
Electron temperature on limiter surface	
Top surface (R=5.53m)	150 eV
Leading edge (R=5.78m)	44 eV
Plasma disruption condition	
Peak energy flux	270 J/cm^2
Time for energy deposition	5 ms
Number per year (average)	42

Table 4 Temperature and thermal stress at top surface of limiter with 10-mm thick tile (Heat flux = 2 MW/m^2)

Tile material	Temp. of tile (°C)		Max. stress intensity (MPa)		
	Max. temp.	Allowable temp.[2]	Tile	Cu	3-Sm of tile[3]
C(Unirr.)	427	400	14	67	20
C(Irr.)	797	400	13	65	20
PG(Unirr.)	205	400	15	68	3
PG(Irr.)	797	400	65	121	3
SiC(Unirr.)[1]	264	1670	176	130	180
SiC(Irr.)	1078	1670	365	180	180
Be(Unirr.)	293	850	123	80	275

(1) High conductivity SiC (BeO rich)

(2) The allowable temperature for C and PG is determined by chemical sputtering, and that for SiC and Be is determined by the vaporization of 0.4 mm/y for duty cycle = 50% and availability = 25%.

(3) 3-Sm of Cu = 120 MPa

Table 5 Temperature and thermal stress at leading edge of limiter with 10-mm thick tile (Heat flux = 0.35 MW/m^2)

Tile material	Temp. of tile (°C)		Max. stress intensity (MPa)		
	Max. temp.	Allowable temp.[2]	Tile	Cu	3-Sm of tile[3]
C(Unirr.)	175	400	8	42	20
C(Irr.)	274	400	7	41	20
PG(Unirr.)	120	400	19	39	3
PG(Irr.)	276	400	29	32	3
SiC(Unirr.)[1]	133	1670	152	78	180
SiC(Irr.)	359	1670	131	77	180
Be(Unirr.)	141	850	22	46	275

(1) High conductivity SiC (BeO rich)

(2) The allowable temperature for C and PG is determined by chemical suputtering, and that for SiC and Be is determined by the vaporization of 0.4 mm/y for duty cycle = 50% and availability = 25%.

(3) 3-Sm of Cu = 120 MPa

Table 6 Allowable thickness and lifetime of tiles at top surface of limiter (Heat flux = 2 MW/m^2)

Tile material	Allowable thickness		Erosion[1] (mm/y)		Lifetime
	Thickness (mm)	Limit	Disruption[2]	Sputtering	(Years)
C(Unirr.)	9	Temp.	0.1	7	1.3
C(Irr.)	4	Temp.	0.1	7	0.6
PG(Unirr.)	<<5	Stress	-	7	Short
PG(Irr.)	<<5	Stress	-	7	Short
SiC(Unirr.)	<5	Stress	1.4	17	<0.3
SiC(Irr.)	<<5	Stress	1.4	17	Short
Be(Unirr.)	∿15	Stress	6.0	10	0.9

(1) Duty cycle = 50%, Availability = 25%, Disruption per year = 42

(2) Erosion assuming all melt layer is lost

Table 7 Allowable thickness and lifetime of tiles at leading edge of limiter (Heat flux = 0.35 MW/m^2)

Tile material	Allowable thickness		Erosion[1] (mm/y)		Lifetime
	Thickness (mm)	Limit	Disruption	Sputtering	(Years)
C(Unirr.)	>20	Temp.	0.1	5	Long
C(Irr.)	15	Temp.	0.1	5	3.0
PG(Unirr.)	<<5	Stress	-	5	Short
PG(Irr.)	<<5	Stress	-	5	Short
SiC(Unirr.)	>20	Stress	1.4	9	Long
SiC(Irr.)	20	Stress	1.4	9	1.9
Be(Unirr.)	>20	Stress	6.0	9	Long

(1) Duty cycle = 50%, Availability = 25%, Disruption per year = 42

(2) Erosion assuming all melt layer is lost

Table 8 Alternative limiter operating conditions

Normal operation	
Total energy to limiter	60 MW
Ion flux	2.95×10^{23}/s
Edge electron temperature	280 eV
Composition of ions (average)	38%D, 55.5%T, 6%He, 0.5%Z
Peak heat flux normal to limiter surface	
Top surface (R = 5.47m)	3 MW/m^2
Leading edge (R = 5.73m)	1 MW/m^2
Peak ion flux normal to limiter surface	
Top surface (R = 5.53m)	1.1×10^{22}/m^2-s
Leading edge (R = 5.73m)	1.2×10^{22}/m^2-s
Electron temperature on limiter surface	
Top surface (R = 5.53m)	150 eV
Leading edge (R = 5.73m)	54 eV
Plasma disruption condition	
Peak energy flux	270 J/cm^2
Time for energy deposition	5 ms
Number per year (average)	42

Table 9 Temperature and thermal stress at top surface of limiter with 10-mm thick tile (Heat flux = 3 MW/m^2)

Tile material	Temp. of tile (°C)		Max. stress intensity (MPa)		
	Max.temp.	Allowable temp.[2]	Tile	Cu	3-Sm of tile[3]
C(Unirr.)	602	400	19	95	20
C(Irr.)	1124	400	18	91	20
PG(Unirr.)	274	400	22	97	3
PG(Irr.)	1124	400	94	172	3
SiC(Unirr.)[1]	362	1670	245	183	180
SiC(Irr.)	1470	1670	490	244	180
Be(Unirr.)	405	850	172	113	275

(1) High conductivity SiC (BeO rich)

(2) The allowable temperature for C and PG is determined by chemical sputtering, and that for SiC and Be is determined by the vaporization of 0.4 mm/y for duty cycle = 50% and availability = 25%.

(3) 3-Sm of Cu = 120 MPa.

Table 10 Temperature and thermal stress at leading edge of limiter with 10-mm thick tile (Heat flux = 1 MW/m^2)

Tile material	Temp. of tile (°C)		Max. stress intensity (MPa)		
	Max. temp.	Allowable temp.[2]	Tile	Cu	3-Sm of tile[3]
C(Unirr.)	358	400	17	105	20
C(Irr.	613	400	15	102	20
PG(Unirr.)	211	400	39	100	3
PG(Irr.)	617	400	70	83	3
SiC(Unirr.)[1]	247	1670	316	165	180
SiC(Irr.)	813	1670	257	184	180
Be(Unirr.)	269	850	48	129	275

(1) High conductivity (SiC (BeO rich)

(2) The allowable temperature for C and PG is determined by chemical sputtering, and that for SiC and Be is determined by the vaporization of 0.4 mm/y for duty cycle = 50% and availability = 25%.

(3) 3-Sm of Cu = 120 MPa.

Table 11 Allowable thickness and lifetime of tiles at top surface of limiter (Heat flux = 3 MW/m^2)

Tile material	Allowable thickness		Erosion[1] (mm/y)		Lifetime
	Thickness (mm)	Limit	Disruption[2]	Sputtering	(Years)
C(Unirr.)	5	Temp.	0.1	7	0.7
C(Irr.)	2	Temp.	0.1	7	0.3
PG(Unirr.)	<<5	Stress	-	7	Short
PG(Irr.)	<<5	Stress	-	7	Short
SiC(Unirr.)	<5	Stress	1.4	17	<0.3
SiC(Irr.)	<<5	Stress	1.4	17	Short
Be(Unirr.)	10	Stress	6.0	10	0.6

(1) Duty cycle = 50%, Availability = 25%, Disruption per year = 42

(2) Erosion assuming all melt layer is lost

Table 12 Allowable thickness and lifetime of tiles at leading edge of limiter (Heater flux = 1 MW/m^2)

Tile material	Allowable thickness		Erosion[1] (mm/y)		Lifetime
	Thickness (mm)	Limit	Disruption[2]	Sputtering	(Years)
C(Unirr.)	12	Temp.	0.1	9	1.3
C(Irr.)	6	Temp.	0.1	9	0.7
PG(Unirr.)	<<5	Stress	-	9	Short
PG(Irr.)	<<5	Stress	-	9	Short
SiC(Unirr.)	<<5	Stress	1.4	16	Short
SiC(Irr.)	<<5	Stress	1.4	16	Short
Be(Unirr.)	7	Stress	6.0	15	0.3

(1) Duty cycle = 50%, Availability = 25%, Disruption per year = 42

(2) Erosion assuming all melt layer is lost

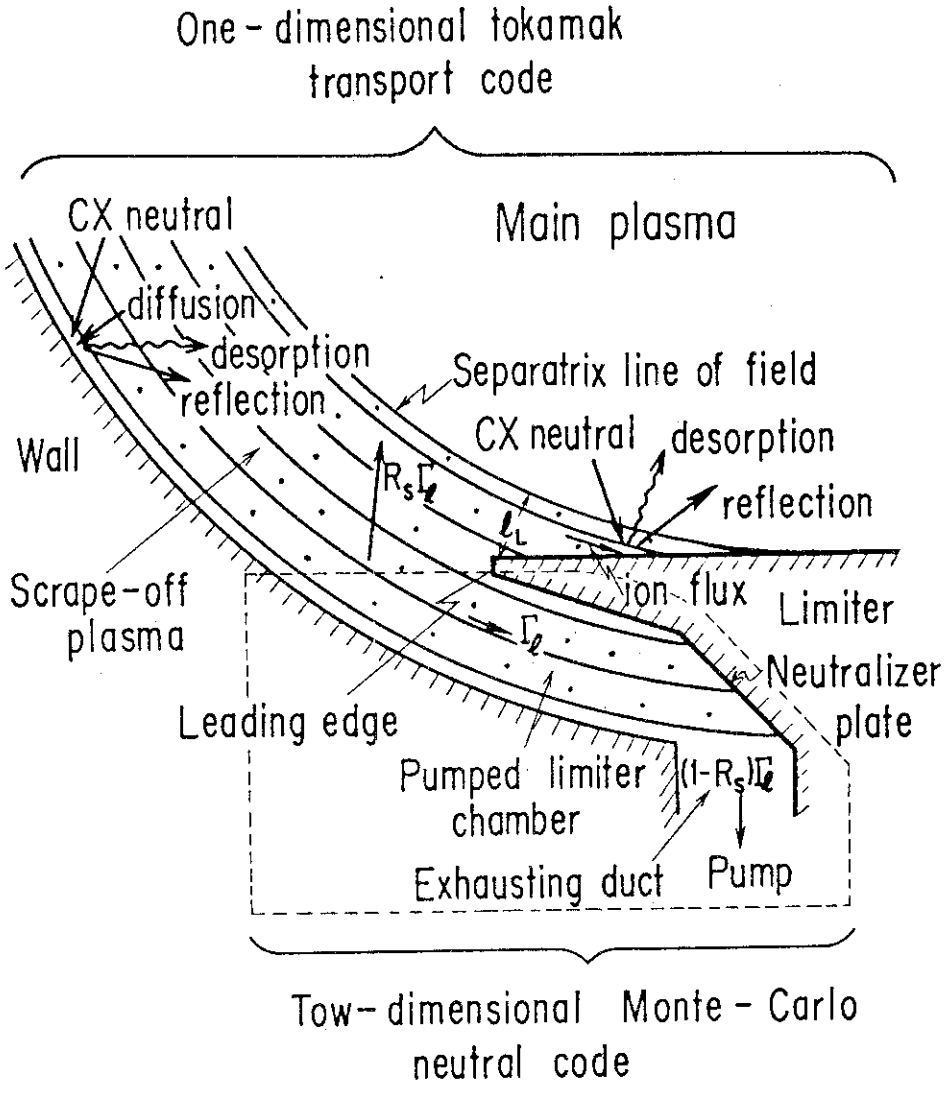

Fig. 1 Schematic drawing of calculational model. Main plasma including scrape-off layer plasma is calculated by one-dimensional tokamak transport code. In pumped limiter chamber, neutral particle behavior is calculated by two-dimensional Monte-Carlo code.

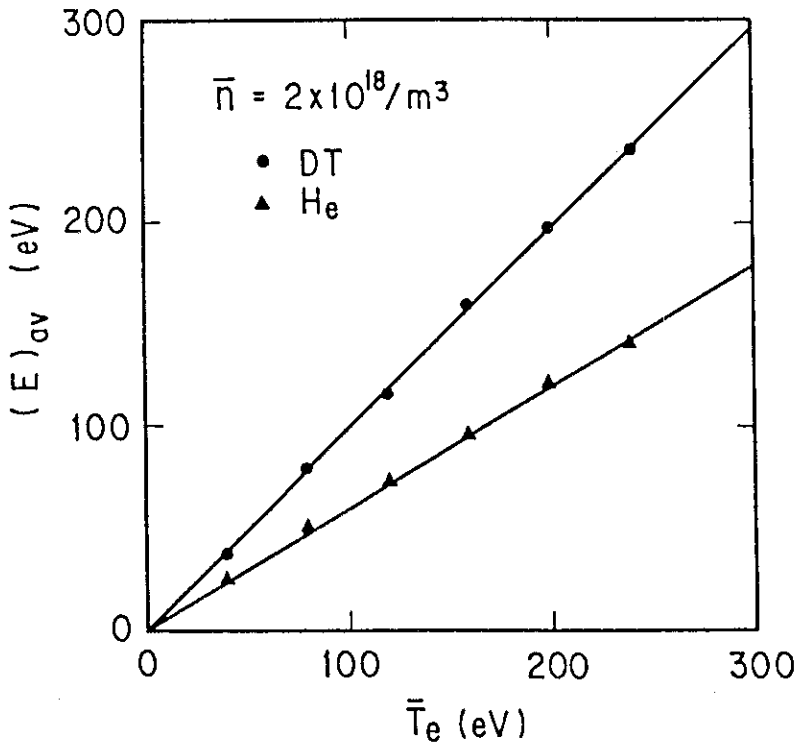

Fig. 2 Average energy of fuel and helium neutral particles, which flow back to the main plasma, calculated by two-dimensional Monte-Carlo neutral code as a function of temperature of scrape-off layer plasma. Density of the scrape-off layer plasma is 2 $\times 10^{18}$ m^{-3}.

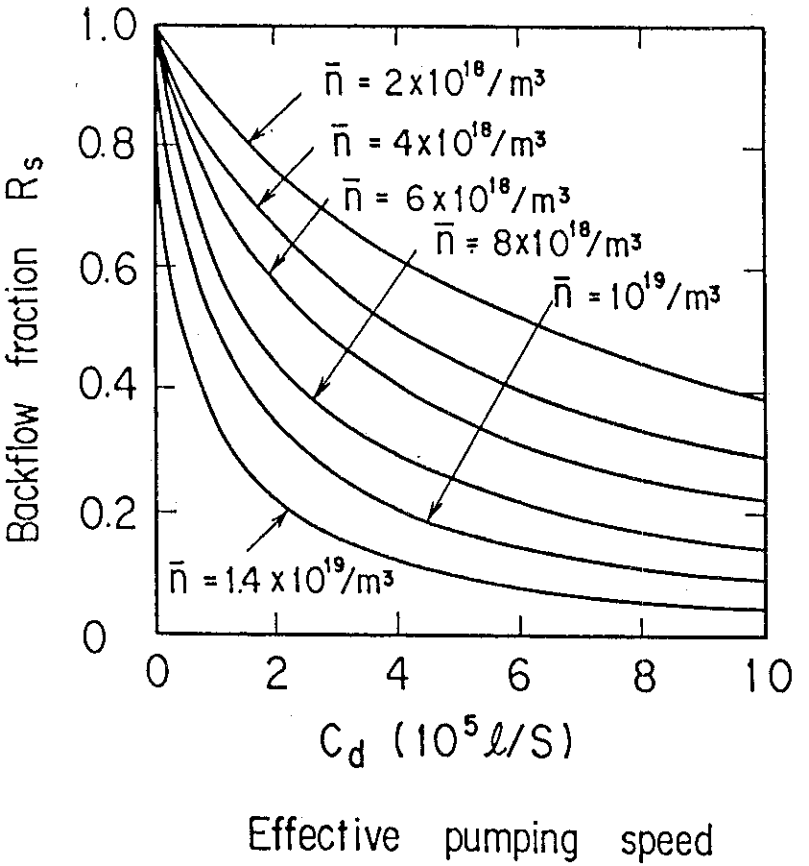

Fig. 3 Backflow fraction R_s vs. effective pumping speed C_d at the entrance of the evacuating duct with density of scrape-off layer plasma as parameters.

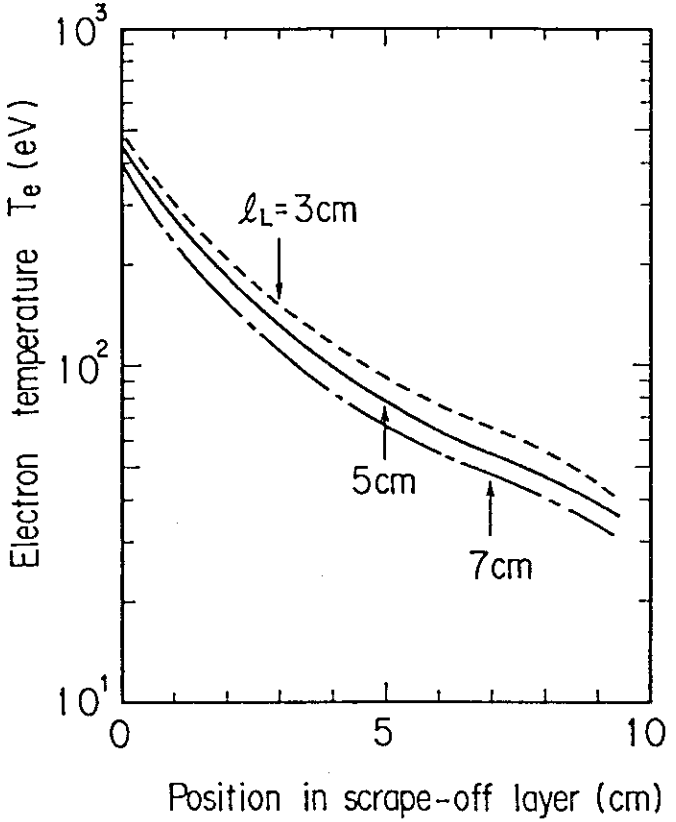

Fig. 4 Profile of electron temperature in scrape-off layer. Pellet injection ① and $R_s = 0.8$ are employed. Arrows indicate the position of leading edge of limiter.

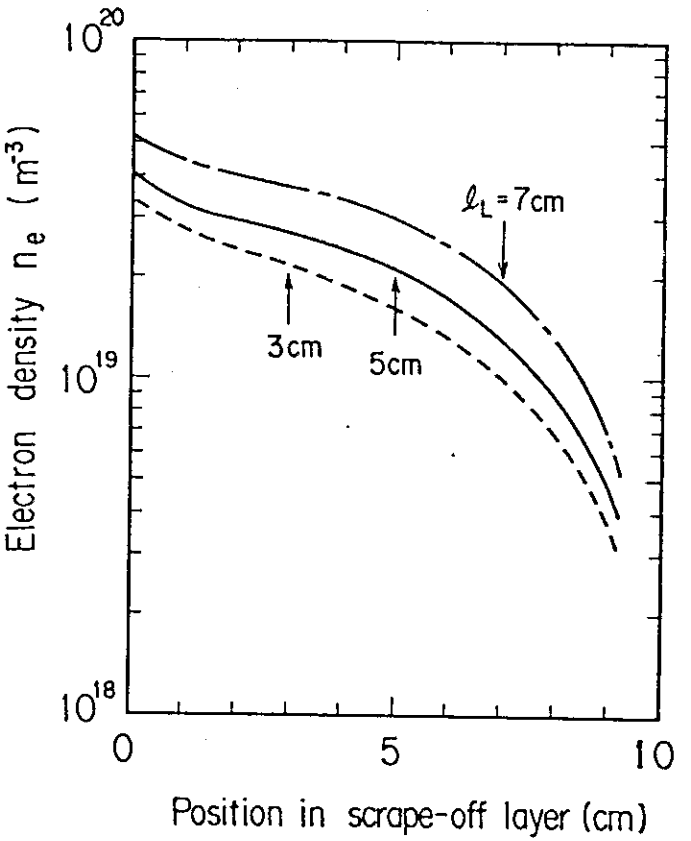

Fig. 5 Profile of electron density in scrape-off layer. Pellet injection ① and $R_s = 0.8$ are employed. Arrows indicate the position of leading edge of limiter.

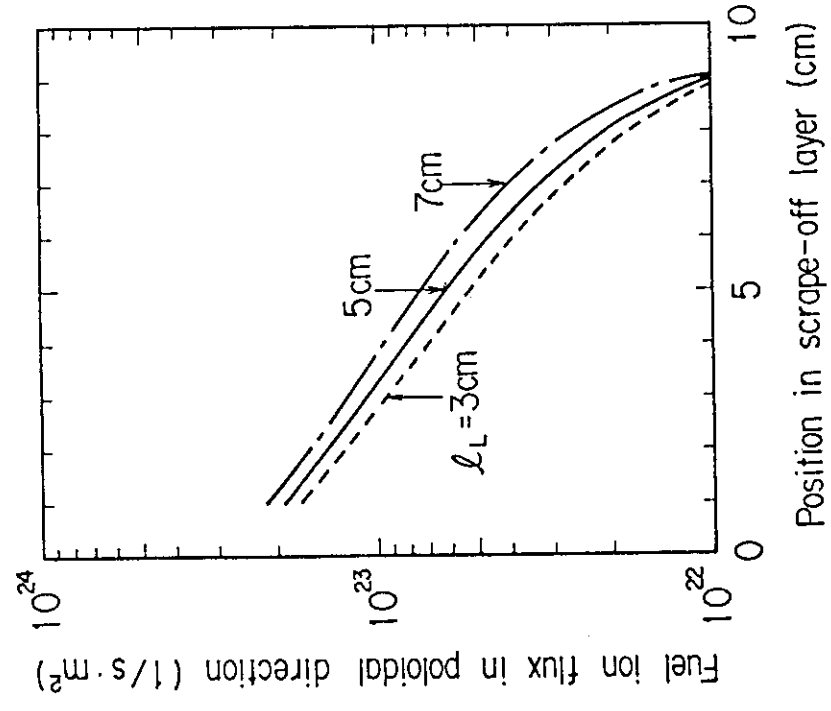

Fig. 6 Profile of fuel particle flux in poloidal direction in scrape-off layer. Pellet injection ① and $R_s = 0.8$ are employed. Arrows indicate the position of leading edge of limiter.

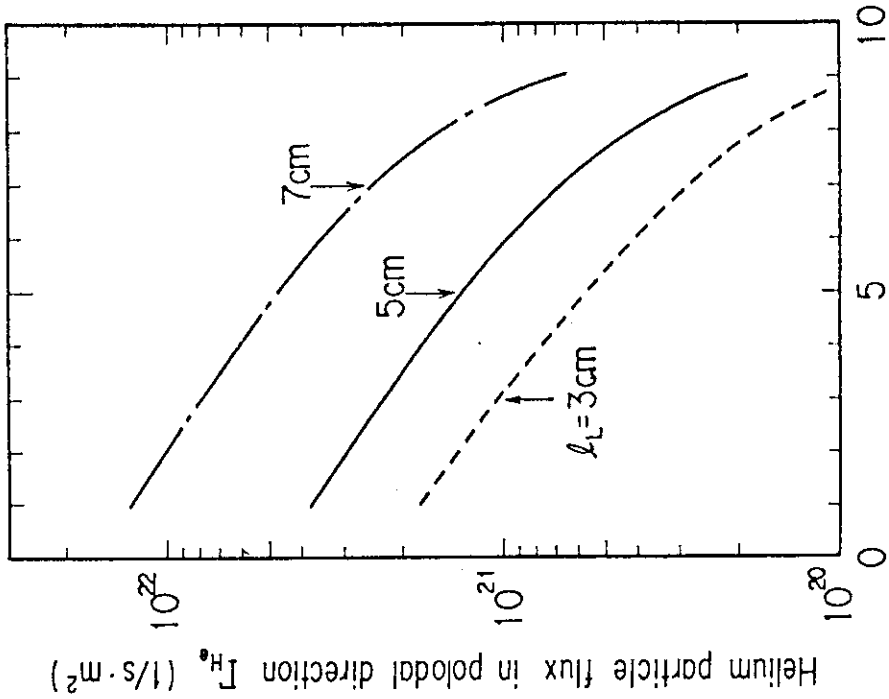

Fig. 7 Profile of helium particle flux in poloidal direction in scrape-off layer. Pellet injection ① and $R_s = 0.8$ are employed. Arrows indicate the position of leading edge of limiter.

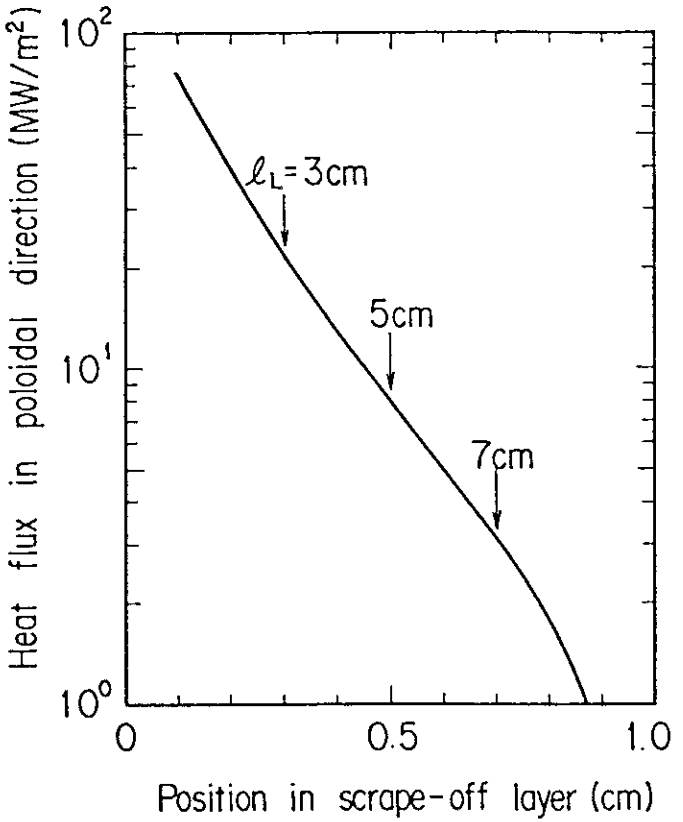

Fig. 8 Profile of total heat flux in poloidal direction in scrape-off layer. Pellet injection ① and R_s = 0.8 are employed. There is on appreciable difference in the profile for various ℓ_L. Arrows indicate the position of leading edge of limiter.

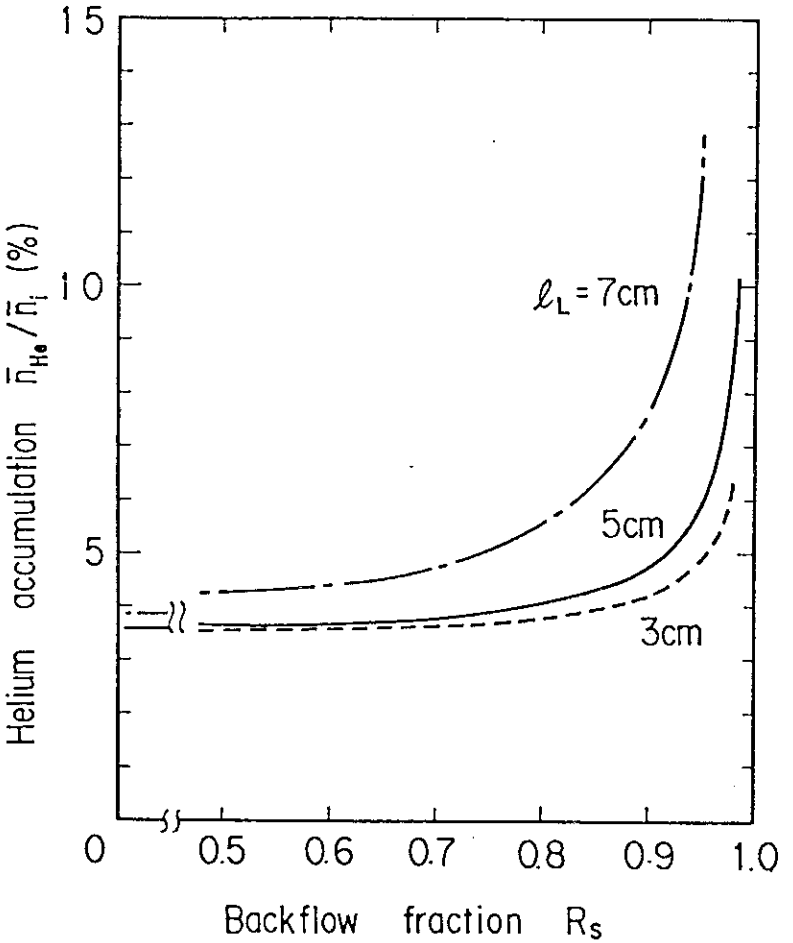

Fig. 9 Helium ash accumulation in main plasma as R_s is varied for ℓ_L = 3, 5 and 7 cm. Fueling is performed by pellet injection ①.

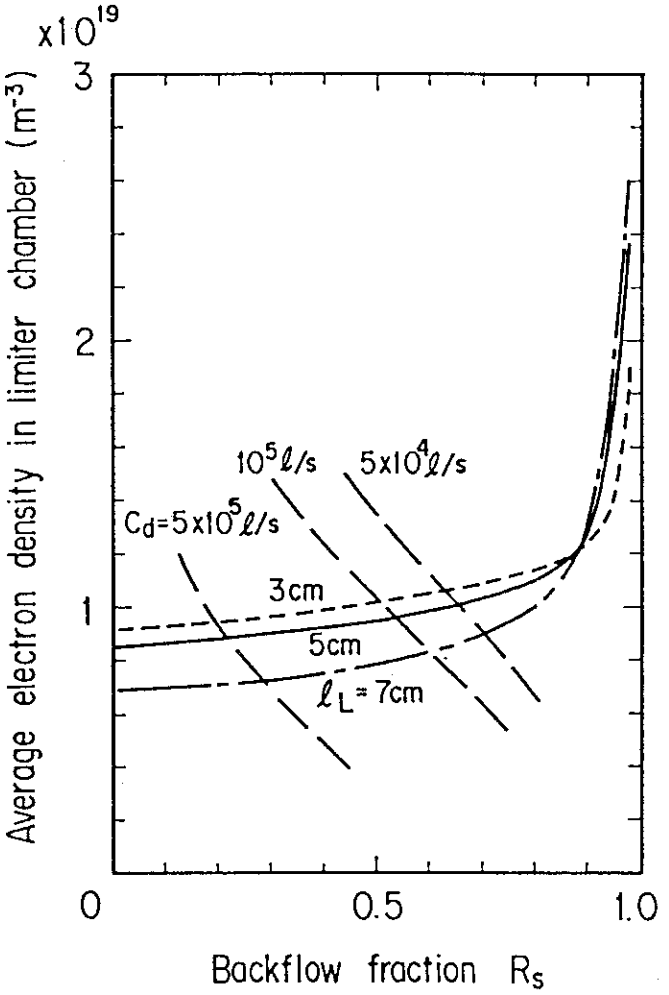

Fig. 10 Average densities in limiter chamber for each ℓ_L as R_s is varied. Relations between plasma density and R_s of Fig. 3 with C_d being fixed are also shown by long broken lines.

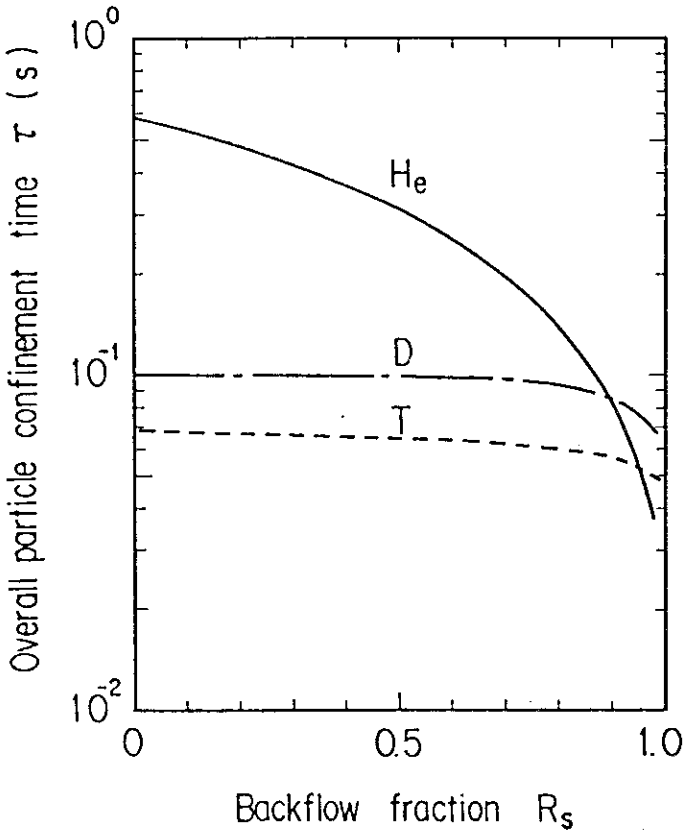

Fig. 11 Overall particle confinement times for deuterium (D), tritium (T) and helium (He) for $\ell_L = 5$ cm. Fueling is performed by pellet injection ①.

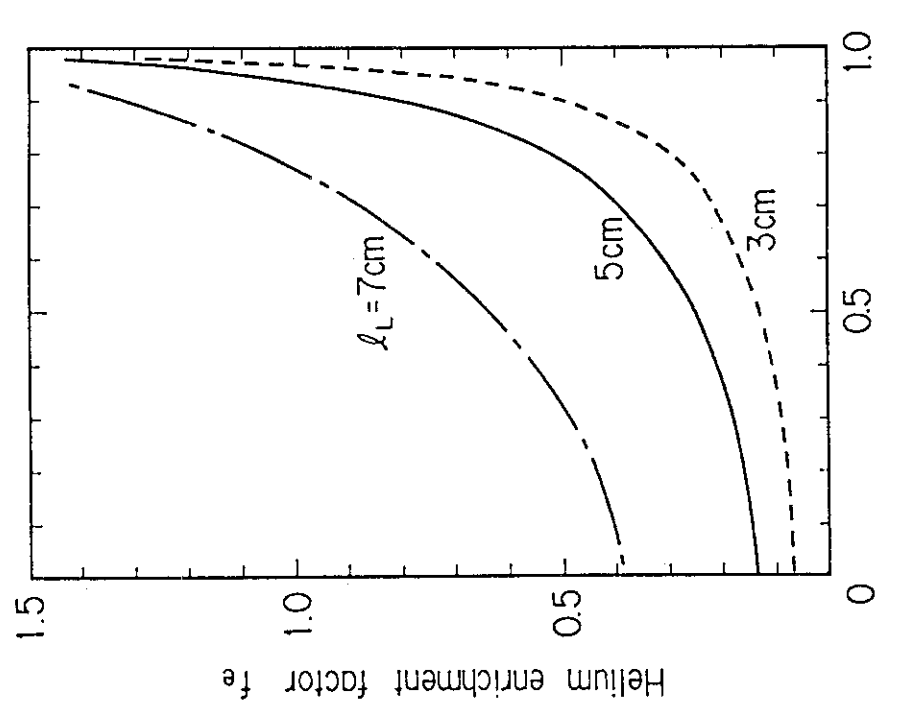

Fig. 12 Helium enrichment factor as R_s is varied for various ℓ_L. Fueling is performed by pellet injection ①.

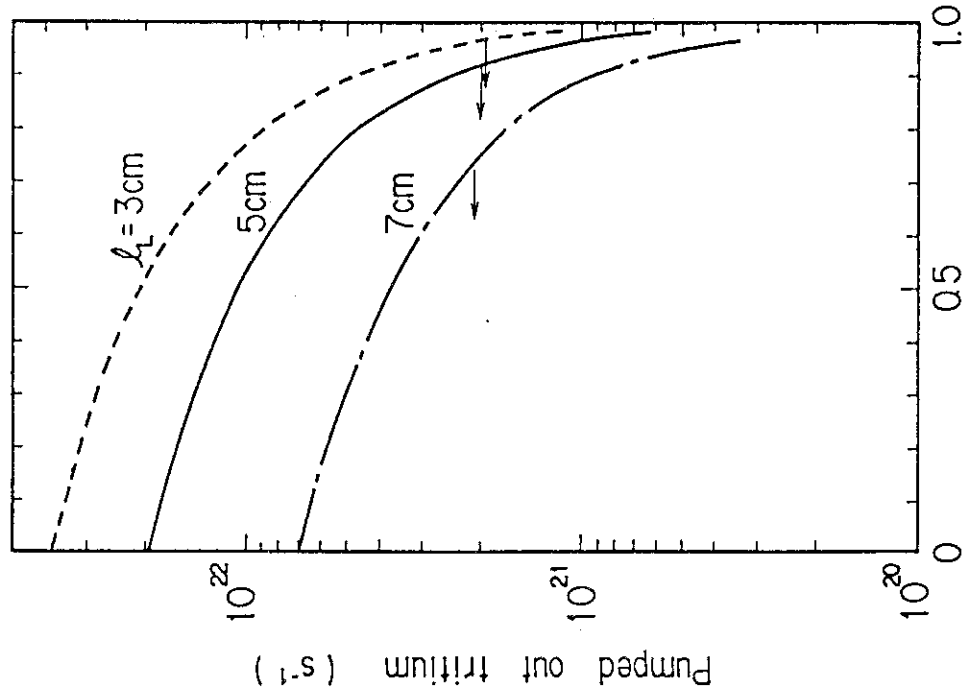

Fig. 13 Absolute amount of tritium pumped out as R_s is varied for various ℓ_L. They are almost the same for all ℓ_L as shown by arrows, if the accumulation is same (5%).

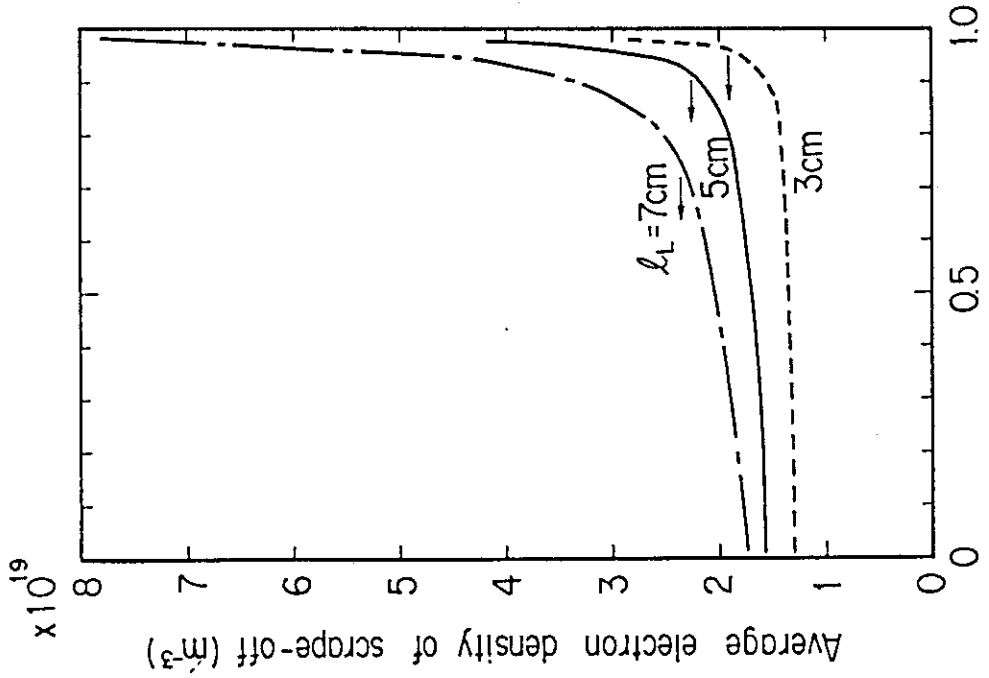

Fig. 15 Average electron density of scrape-off layer plasma as R_s is varied for various ℓ_L. Fueling is performed by pellet injection ①.

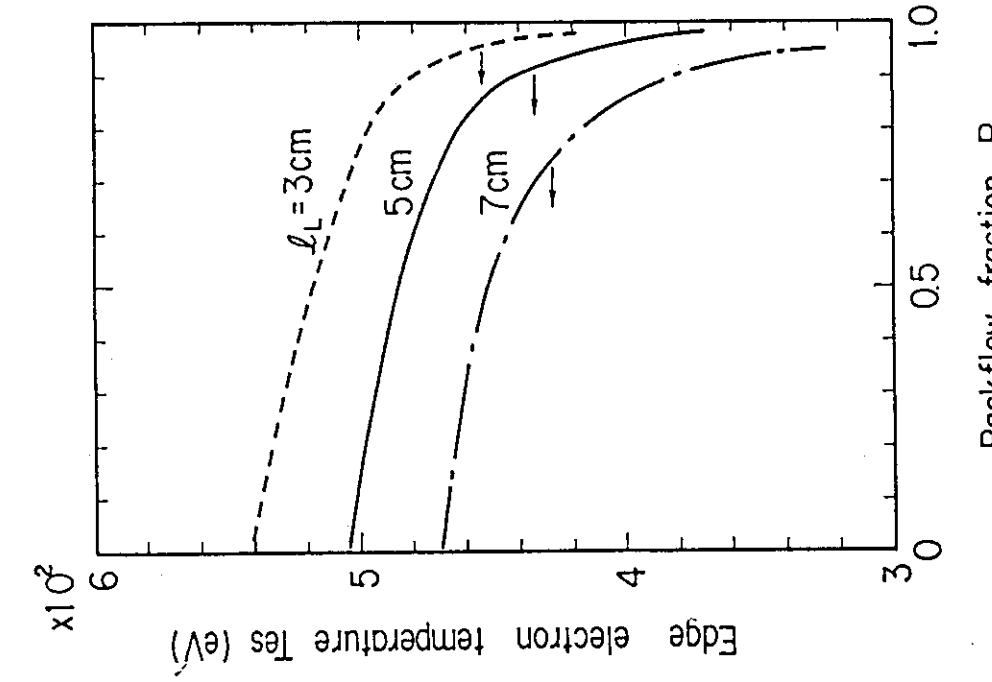

Fig. 14 Electron temperature at separatrix as R_s is varied for various ℓ_L. Fueling is performed by pellet injection ①.

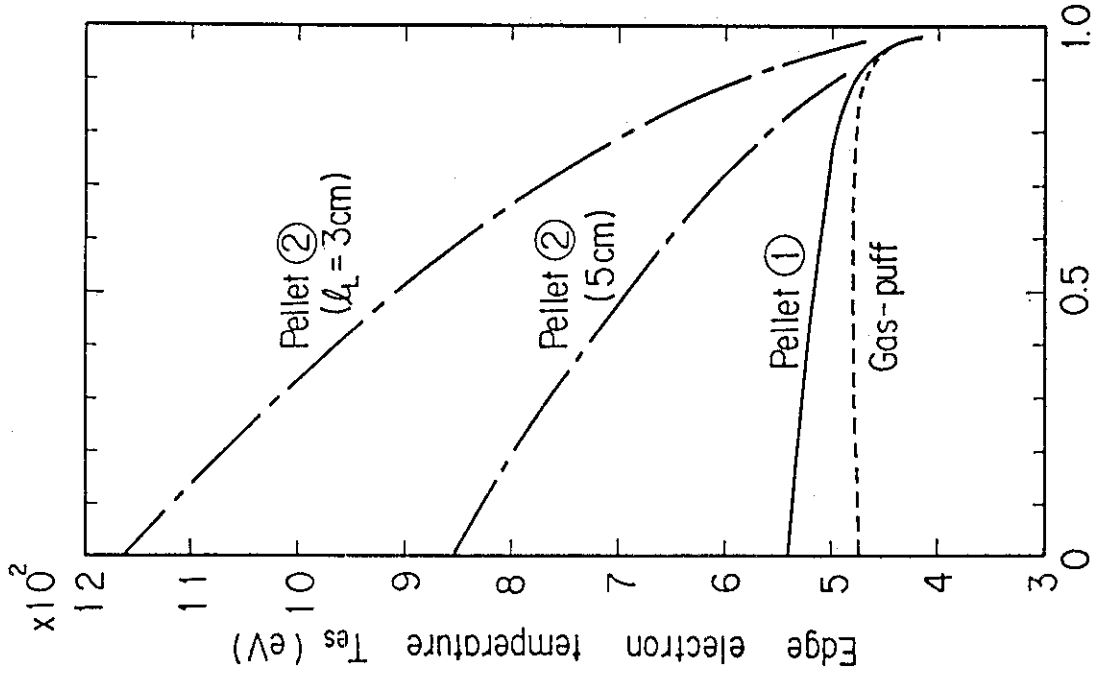

Fig. 17 Electron temperature at separatrix by various fueling method for ℓ_L = 3 cm (pellet ① and ② and gas-puffing) and ℓ_L = 5 cm (pellet ② as R_s is varied.

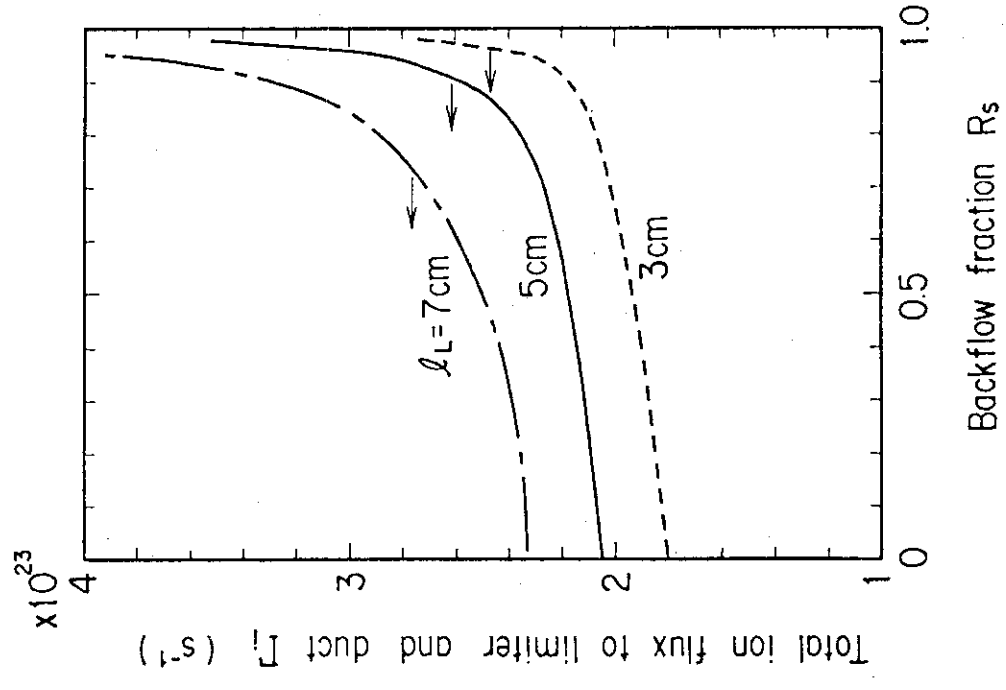

Fig. 16 Total ion particle flux to limiter and chamber as R_s is varied for various ℓ_L. Fueling is performed by pellet injection ①.

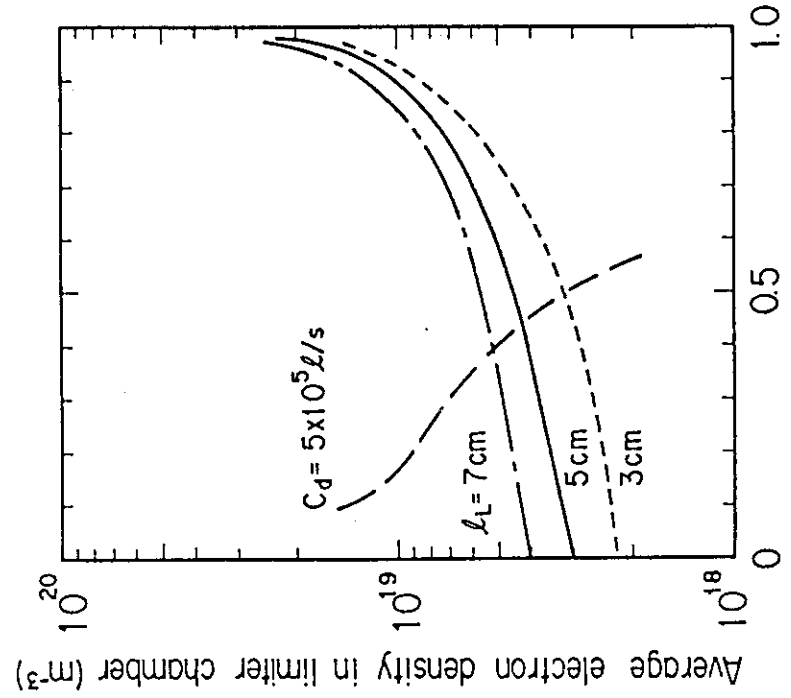

Fig. 19 Average electron density in limiter chamber for various ℓ_L as R_s ia varied. Fueling is performed by pellet injection ②. Relation between plasma density and R_s with $C_d = 5 \times 10^5$ ℓ/s is also shown by long broken line.

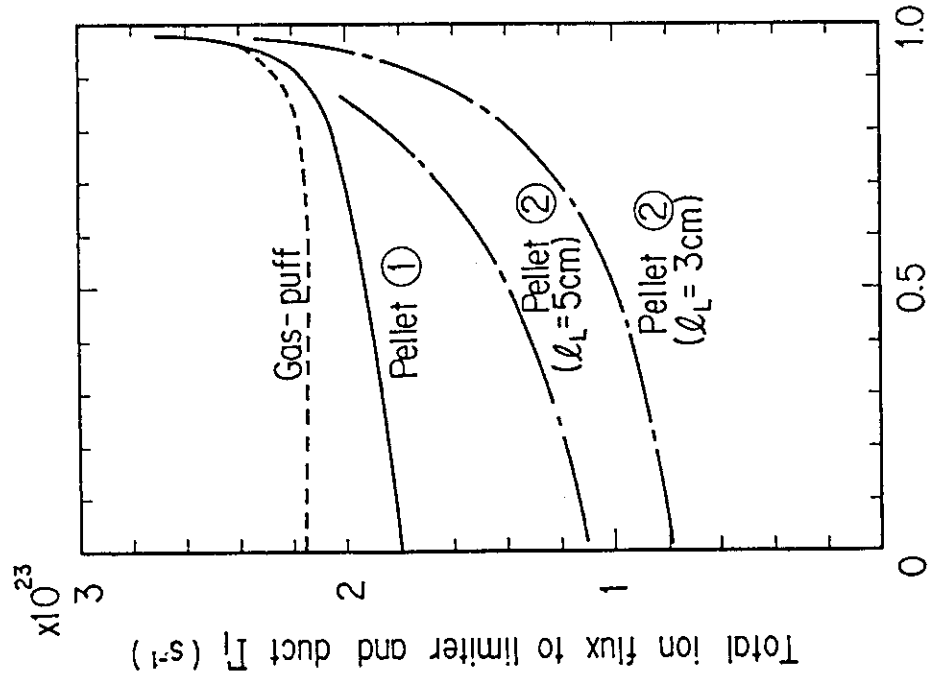

Fig. 18 Total ion particle flux to limiter and chamber by various fueling methods for ℓ_L = 3 cm (pellet ① and ② and gas-puffing) and ℓ_L = 5 cm (pellet ②) as R_s is varied.

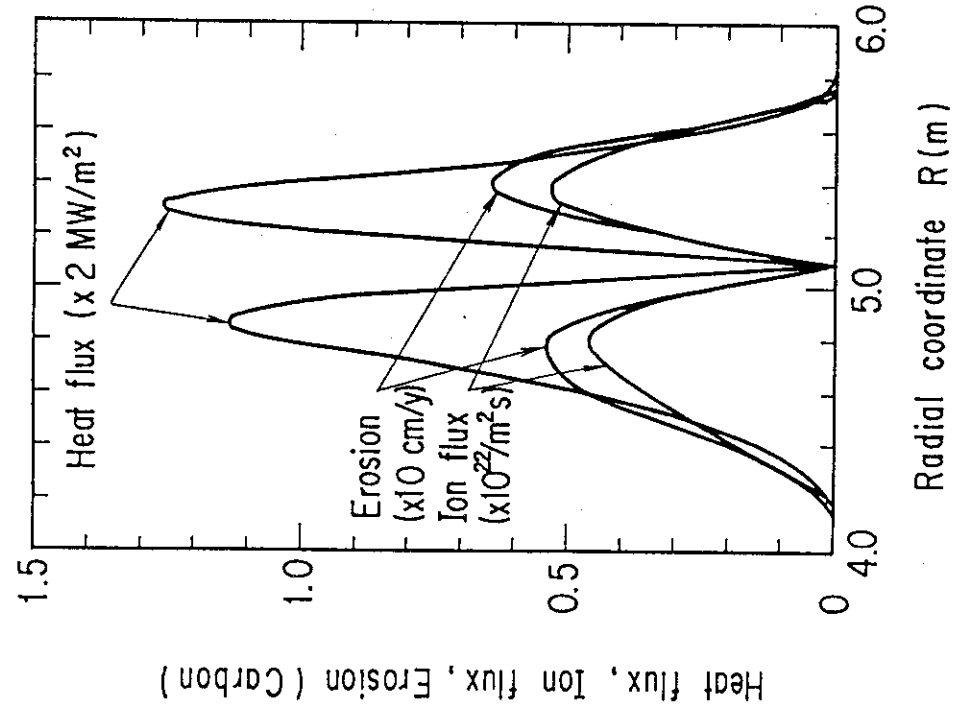

Fig. 20 Distributions of heat and ion particle flux and erosion on carbon limiter surface for Case I.

Fig. 21 Distributions of heat and ion particle flux and erosion on carbon limiter surface for Case III.

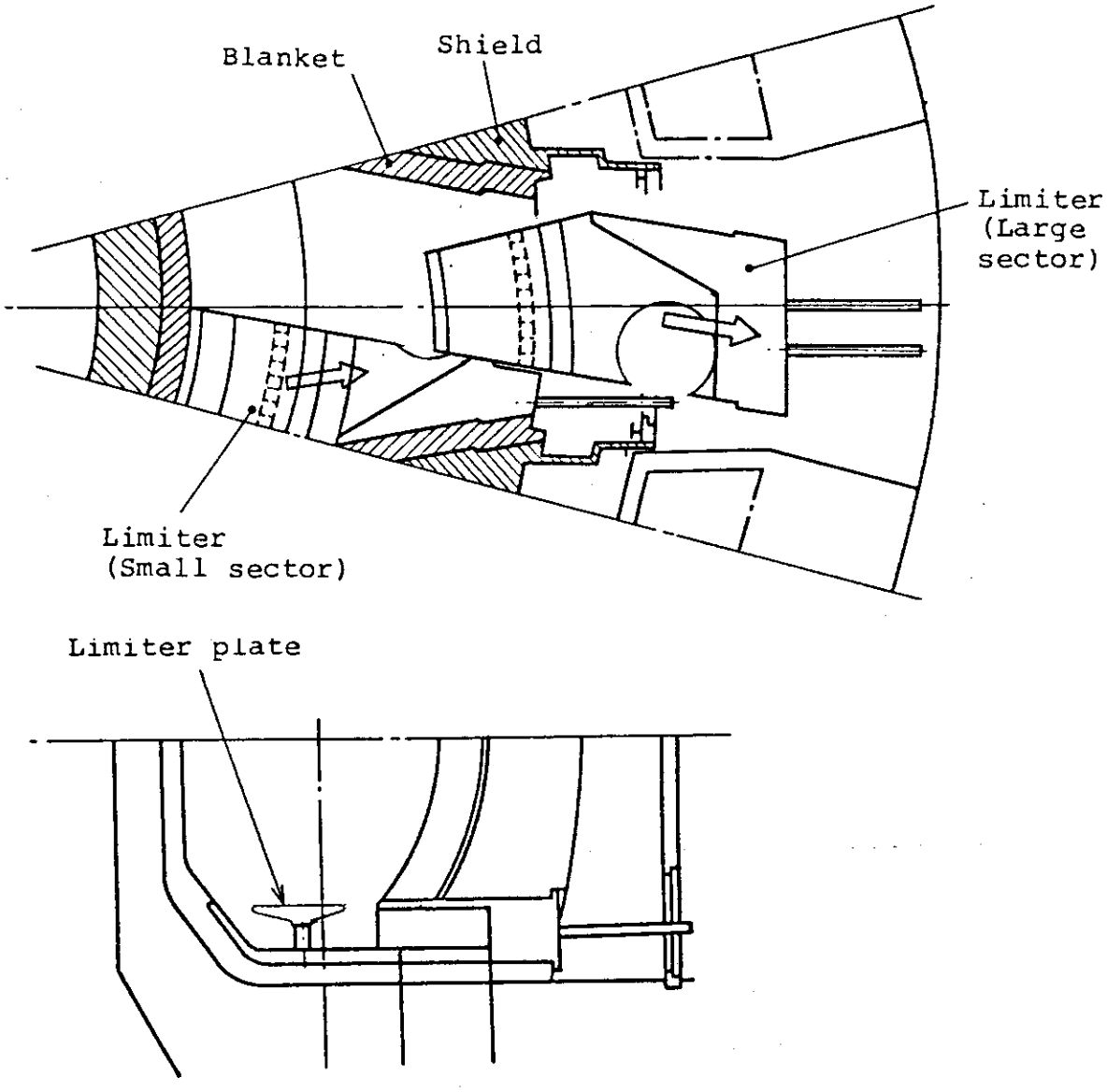

Fig. 22 Limiter replacement concept